Research Paper

GEOSPHERE

GEOSPHERE; v. 14, no. 6

https://doi.org/10.1130/GES01687.1

13 figures; 2 tables

CORRESPONDENCE: nate.onderdonk@csulb.edu

CITATION: Onderdonk, N., McGill, S., and Rockwell, T., 2018, A 3700 yr paleoseismic record from the northern San Jacinto fault and implications for joint rupture of the San Jacinto and San Andreas faults: Geosphere, v. 14, no. 6, https://doi.org/10.1130/GES01687.1.

Science Editor: Raymond M. Russo

Received 26 February 2018
Revision received 11 June 2018
Accepted 13 August 2018

A 3700 yr paleoseismic record from the northern San Jacinto fault and implications for joint rupture of the San Jacinto and San Andreas faults

N. Onderdonk[1], S. McGill[2], and T. Rockwell[3]

[1]Department of Geological Sciences, California State University–Long Beach, 1250 Bellflower Boulevard, Long Beach, California 90840, USA
[2]Department of Geological Sciences, California State University–San Bernardino, 5500 University Parkway, San Bernardino, California 92407, USA
[3]Department of Geological Sciences, San Diego State University, 5500 Campanile Drive, San Diego, California 92182, USA

ABSTRACT

The San Andreas and San Jacinto faults are the primary plate-boundary structures in southern California and present a large earthquake hazard for the region. They approach each other in the Cajon Pass area between the San Gabriel and San Bernardino Mountains, where the northern end of the San Jacinto fault forms a 2-km-wide releasing step with the San Andreas fault. In this study, we used paleoseismic data from sites on the San Jacinto and San Andreas faults near their juncture to evaluate spatial and temporal patterns of surface rupture between these major structures of the North American–Pacific transform plate boundary. We present a new 3700 yr paleoseismic record from the northern San Jacinto fault at Mystic Lake, where trench excavations exposed evidence for at least 16 surface ruptures. A sedimentary gap in our trench exposures separates three ruptures in the oldest part of the record from 13 ruptures during the past 2000 yr. For the past 2000 yr, the mean recurrence times varied from 86 to 312 yr, with a mean recurrence interval of 160 yr. This rate of surface rupture is roughly equal to that of the southern San Andreas fault south of the Cajon Pass juncture, but it is half that of the San Andreas fault north of the juncture, indicating that coseismic strain on the San Andreas fault is split between the southern San Andreas and San Jacinto faults south of Cajon Pass. Comparison of the past 2000 yr of the Mystic Lake record to similar paleoseismic records from nearby sections of the San Andreas fault suggests that: (1) the current open interval on these two faults in the study area is longer than their average recurrence intervals, but that similar intervals of quiescence have occurred in the past 2000 yr; (2) the San Andreas and San Jacinto faults have probably ruptured together multiple times in the past 2000 yr; and (3) a joint rupture of the San Jacinto fault with the Mojave section of the San Andreas fault may be a more likely source of a major earthquake in southern California than a rupture on the San Andreas fault from the Mojave segment to the southern end of the fault.

INTRODUCTION

The interaction between major faults in the San Andreas fault system is a primary concern for earthquake hazards in California, and it is crucial to understanding the dynamics of the plate boundary. Continental plate boundaries typically consist of multiple faults that accommodate the relative motion between lithospheric plates. Individual faults in these plate-boundary systems can link to each other via steps or splays, and the size and lateral extent of earthquake ruptures depend on whether or not ruptures can propagate through these junctions. It is therefore critical to understand how neighboring faults interact in order to understand, and forecast, earthquake behavior within a fault system. The relative abundance of paleoseismic data from faults in the San Andreas fault system in California presents an opportunity to study the degree and nature of interaction between separate faults on time scales of hundreds to thousands of years. In this paper, we present new paleoseismic data from the northern San Jacinto fault in southern California that we compare with similar data from the adjacent San Andreas fault to evaluate the 2000 yr history and spatial pattern of earthquake ruptures on these two faults near their junction.

Geologic and geodetic data show that along the North American–Pacific plate boundary in central California, the San Andreas fault accommodates ~70% of the total displacement across the boundary (e.g., Thatcher, 1979; Sieh and Jahns, 1984; Prescott et al., 2001). In southern California, however, the ~35 mm/yr late Quaternary slip rate on the Mojave section of the San Andreas fault (e.g., UCERF3 appendix B *in* Dawson and Weldon, 2013) decreases to the southeast though the Cajon Pass to only 7–16 mm/yr along the San Bernardino section of the San Andreas fault (Fig. 1; McGill et al., 2015, 2013; Spinler et al., 2010). The San Jacinto fault diverges southward from the San Andreas fault in the Cajon Pass area and makes up for most of the missing slip rate, with a slip rate of 13–18 mm/yr (McGill et al., 2015; Onderdonk et al., 2015; Blisniuk et al., 2013). Displacement must be transferred between the San Jacinto fault and San Andreas fault across a stepover between the two faults at the north end of

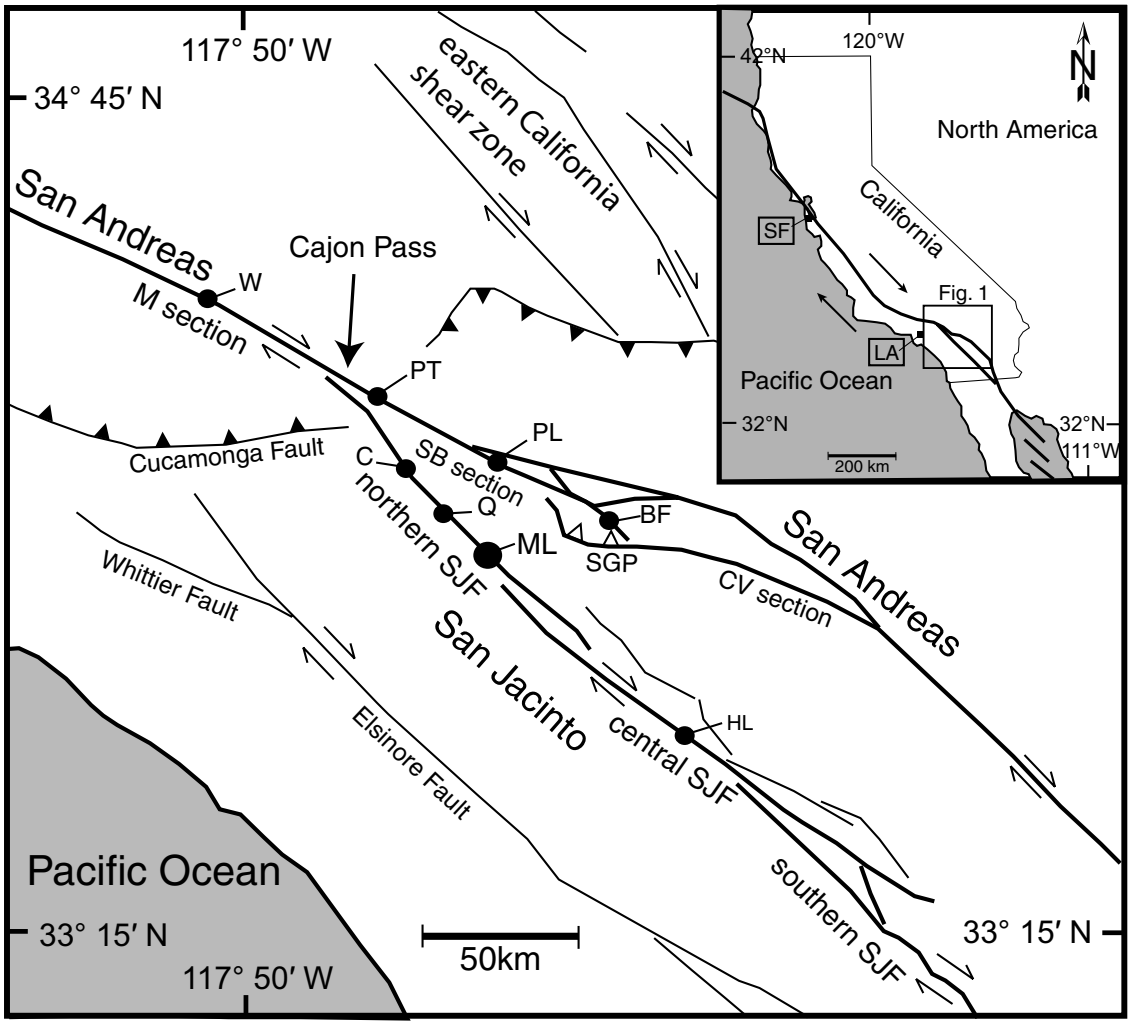

Figure 1. Simplified fault map of southern California with major faults (black lines), and recently dominant strands of the San Andreas fault and San Jacinto fault (SJF) in bold. Teeth are shown on the hanging wall of reverse faults in the Transverse Ranges. Dots indicate paleoseismic sites (BF—Burro Flats, C—Colton, HL—Hog Lake, ML—Mystic Lake, PL—Plunge Creek, PT—Pitman Canyon, Q—Quincy, W—Wrightwood). The San Gorgonio Pass (SGP), Mojave section (M section), San Bernardino section (SB section), and Coachella Valley section (CV section) of the San Andreas fault are labeled. Inset map shows location within California, with the cities of San Francisco (SF) and Los Angeles (LA) for reference.

the San Jacinto fault in the Cajon Pass (i.e., Morton and Matti, 1993; Machette et al., 2004; McGill et al., 2013), but it is not known whether this occurs only as interseismic strain accommodation, or if the two faults have ruptured together. Anderson et al. (2003) used both static and dynamic stress modeling to infer that a rupture on the northern San Jacinto fault will increase Coulomb stress on the Mojave segment of the San Andreas fault and possibly lead to simultaneous rupture. They also modeled a southward-propagating rupture on the Mojave section of the San Andreas fault and showed that resultant rupture on the San Jacinto fault was possible. Other studies (Sanders, 1993; Pollitz and Sacks, 1992) have suggested that historic earthquakes on the San Jacinto fault have been triggered by stress changes due to the A.D. 1857 event on the Mojave section of the San Andreas fault. Grant Ludwig et al. (2015) showed that the presence of precariously balanced rocks near the juncture of the San Jacinto fault and San Andreas fault is more consistent with the lower ground motions expected from joint rupture of the San Jacinto fault and Mojave section of the San Andreas fault than from a rupture passing through the area on the San Andreas fault. This led them to hypothesize that most ruptures in the area initiate at, terminate at, or pass through the stepover between the

San Jacinto fault and San Andreas fault. Dynamic rupture modeling of the San Andreas fault–San Jacinto fault junction by Lozos (2016) supported this idea and showed that historic and paleoseismic evidence for the A.D. 1812 earthquake on the San Andreas fault is best explained by joint rupture of the San Jacinto fault and San Andreas fault during that event. Here, we show that paleoseismic data from the past 2000 yr strongly support the hypothesis of joint rupture and suggest that some ruptures during this time period have passed through the step between the San Andreas fault and San Jacinto fault. We propose that this scenario is more likely than a similarly large rupture involving the entire southern San Andreas fault, based on the fault zone geometries and earthquake histories of the two faults.

METHODS

Our new paleoseismic data were collected from fault trenches excavated across the Claremont strand of the northern San Jacinto fault at Mystic Lake (Fig. 1). The Mystic Lake paleoseismic site is a 400-m-wide by 600-m-long sag that developed due to subsidence and periodic ponding of water against scarps that formed during surface ruptures (Fig. 2). Initial trenching at the site (trenches T1, T2, T3, T4) was done in 2009 to precisely locate the primary active fault strand (fault A at the southwestern side of the sag), and to evaluate the relative activity of three additional fault strands (B, C, and D) that form scarps bounding the northeastern side of the sag. Three additional trenches (T5, T6, T7) were excavated in 2010 to a depth of 1.5 m across fault A to provide additional exposures and identify the best stratigraphic location along the primary active fault strand. These shallow trenches exposed evidence for seven earthquakes since A.D. 500 (Onderdonk et al., 2013), and cone penetrometer testing across the sag documented the progressive growth of the sag over the past 7000 yr (Marliyani et al., 2013). Here, we present and discuss data from additional deeper trenches that were excavated in the same location as trench 6 (Fig. 2), where the stratigraphy was preserved the best along the fault. We excavated a 4-m-deep trench in 2012 (T8), and a 5.5-m-deep trench in 2013 (T9). Both trenches were benched with 1.5–1.75-m-tall bench walls (Fig. 3). The trench exposures allowed us to significantly refine the timing of the previously documented earthquakes with radiocarbon dating of additional samples, and extend the paleoseismic record farther back in time to ca. 1700 B.C.

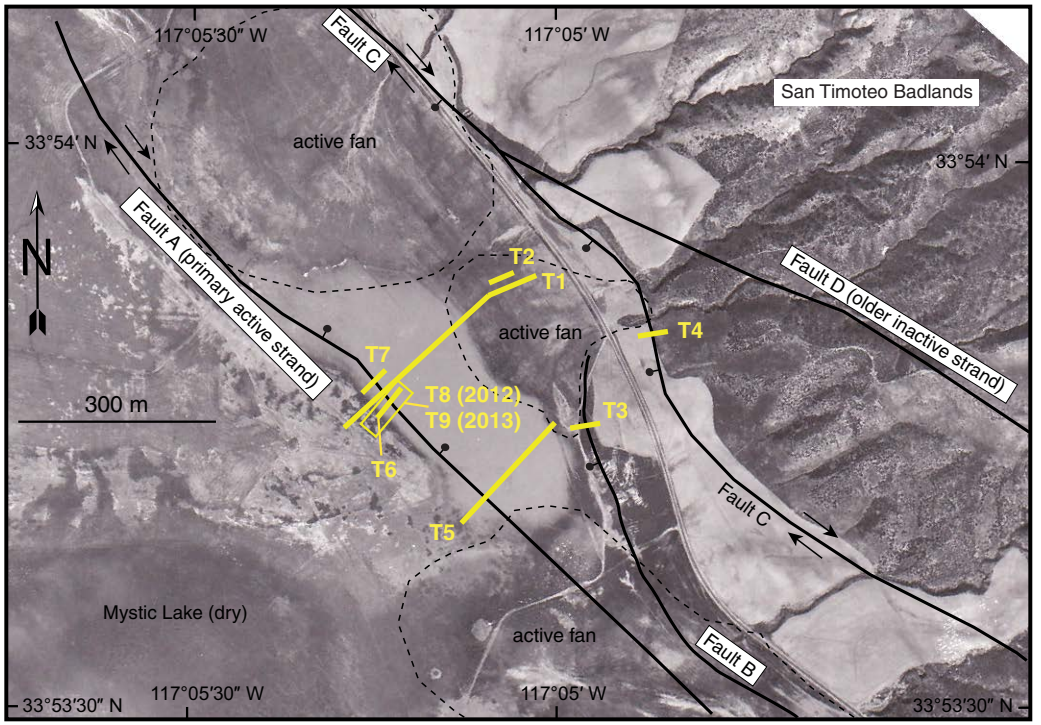

Figure 2. Faults (black lines), and trenches (yellow lines) of the Mystic Lake paleoseismic site mapped on a 1940 air photo. Upper-right side of the photo shows the higher topography of the San Timoteo Badlands and associated canyons that drain into the lower elevations of Mystic Lake at the lower-left corner of the photo. Note the water (lighter gray) that is filling the sag on the northeast side of fault A at the time the photograph was taken; this sag depression is now completely filled with sediment. The outlines of active fans are shown as dashed black lines. Trenches 1 through 7 were excavated in 2009 and 2010 (detailed results in Onderdonk et al., 2013), and trenches 8 and 9 were excavated in 2012 and 2013, respectively.

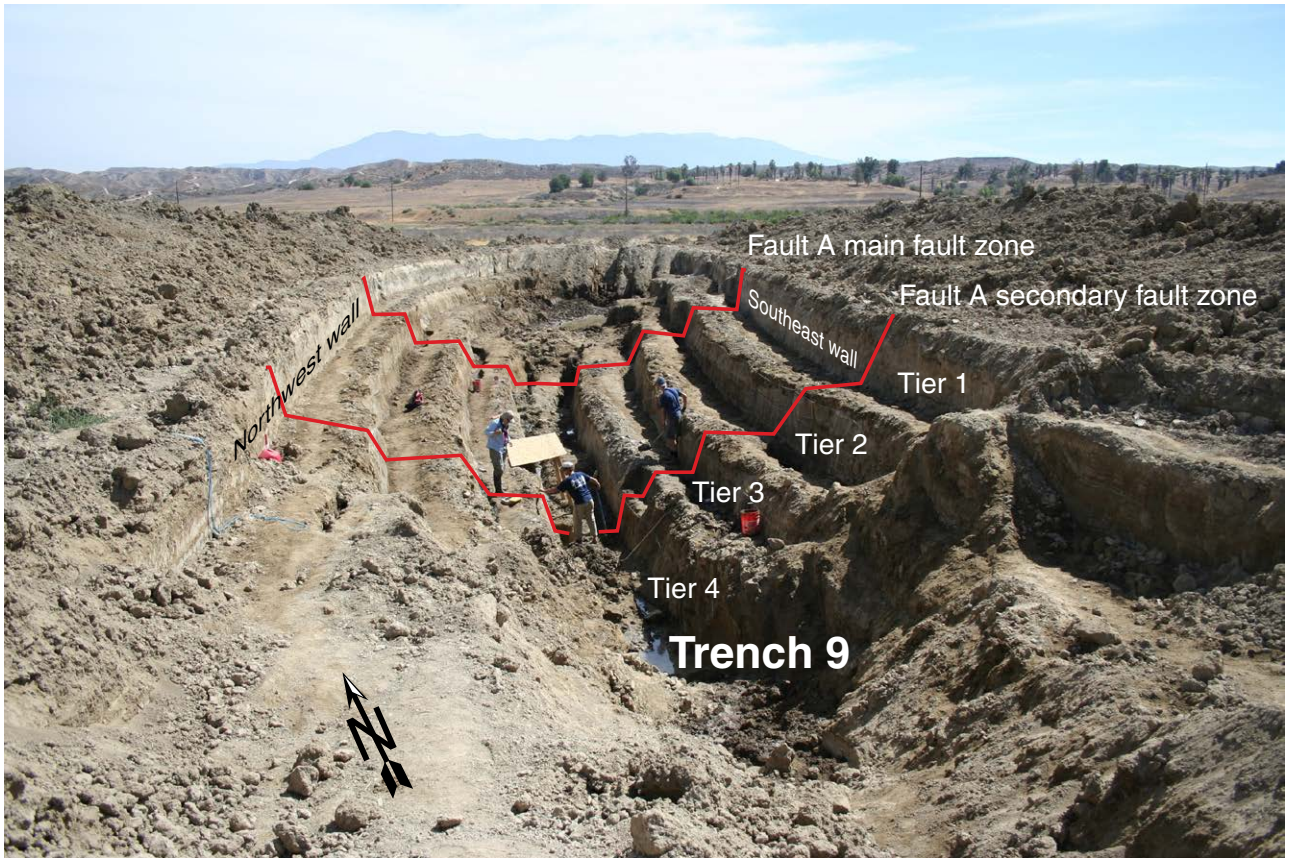

Figure 3. View looking northeast at trench 9 showing benched excavation across fault A. The maximum depth of the trench was 5.5 m in the lowest bench.

Trench walls were scraped and cleaned by hand before a string grid was set up to divide the exposure into 1-m-wide by 0.5-m-tall panels. Stratigraphic units were identified, named, traced along the trench, and correlated with known units exposed in previous trenches. All trench panels were photographed and then digitally assembled into mosaics. Stratigraphic and structural relationships were then described and drawn onto the printed photo mosaics in the field. Datable material was collected and cataloged, and the locations were marked on the trench walls. Over 700 samples were collected for radiocarbon dating, and 118 of these were dated at the Keck Carbon Cycle Accelerator Mass Spectrometry Program at the University of California, Irvine (Table 1). Several models of the stratigraphic unit ages were developed and evaluated based on the dated samples and their relative stratigraphic position. Most of the samples collected were detrital charcoal, so there was an unknown amount of time between the formation of the charcoal during a brush fire and deposition of the charcoal into the stratigraphic section. Consequently, a stratigraphic layer is equal to or younger than the charcoal it contains. We therefore assumed that the youngest charcoal age from each layer provides the closest approximation of the age of that layer, and that radiocarbon samples with ages that are older than samples in underlying units do not represent the true age of the unit that contains them. Using these assumptions, we eliminated almost half of the dated samples, and our stratigraphic model is based on 70 samples (Table 1). An event history for the site was then determined using OxCal software version 4.3 (Bronk Ramsey, 2009), which calculates the probability density functions of radiocarbon sample ages and the event ages based on the dendrochronologically calibrated radiocarbon curve of Reimer et al. (2013).

TABLE 1. RADIOCARBON DATES

Events	Unit	Sample no.	Trench panel*	^{14}C age (yr B.P.)	±1σ
Event 0	Top of 10				
	10	238	63	Modern	
Event 1	Top of 100				
A.D. 1744 to A.D. 1853	100-200	T7-13	18	105	15
Mean = A.D. 1823	100-200	T6-64	17	120	15
	100-200	T7-44	18	130	15
	100-200	T7-43	5	620	15
	100	T7-26	15	1740	90
	190	T1-214	16	355	20
Event 2	Top of 200				
A.D. 1665 to A.D. 1729	200	T1-219	33	40	20
Mean = A.D. 1690	200	T1-7	E1	370	20
	230	T1-210	16	195	20
	240	T1-55	E20	300	20
	250	T1-93p	E57	195	20
	270	T7-1	2	295	15
	290	T1-220	34	670	90
	290	T1-125	E67	345	20
	290	T7-4	4	355	20
	290	T1-65	E27	375	20
	290	T1-208	16	625	20
Event 3	Top of 300				
A.D. 1520 to A.D. 1610	300	T1-5p	E1	370	20
Mean = A.D. 1568	310	T1-221	34	820	20
	320	T1-92p	E56	325	20
	320-340	T7-9	9	325	15
	340	T1-51	E20	390	20
	360	T7-3	3	340	15
	370	T1-212	17	1310	20
	370	T1-209	16	1095	20
	370	T1-226	49	865	20
	370	T6-49	12	440	15
	370	T6-48	12	445	15
	370	T6-52	14	1210	15
	390	T7-7	11	475	15
Event 4	Top of 400				
A.D. 1434 to A.D. 1450	400	T6-22	8	545	15
Mean = A.D. 1442	400	T6-25	8	1120	15
	400	T8-400s	Seed from bulk sample	320	15
	400	T6-46	11	480	30
	420	T8-420ch	Charcoal from bulk sample	460	20
	430	T6-50	12	410	15
	450	T6-42	11	1310	60
	480	T6-45	11	785	15
	480	T8-33	SE Tier M 33	1105	20
	400	T1-244	67	(–890)	90

(*continued*)

TABLE 1. RADIOCARBON DATES (*continued*)

Events	Unit	Sample no.	Trench panel*	^{14}C age (yr B.P.)	±1σ
Event 5	Top of 500				
A.D. 1231 to A.D. 1276	500-520	T1-302	50	740	15
Mean = A.D. 1258	500	T8-500ch1	Charcoal from bulk sample	885	20
	500	T8-500ch2	Charcoal from bulk sample	870	15
	500	T8-500s	Seed from bulk sample	875	15
	500	T1-301	50	890	20
	520	T6-61	16	1240	15
	530	8-66	SE Tier M 28	1140	25
	530	T6-54	14	1045	15
	540	T6-60	16	1120	15
	540	8-32	SE Tier M 32	995	30
	540-500	T6-53	14	2080	60
	550	T8-81	SE Tier M 34	1200	20
	560a	T6-55	14	2160	80
	560a	T6-56	14	1185	15
	560	8-85	SE Tier M 32	Dissolved in pretreatment	
	560?	T1-227	50	960	25
Event 6	Top of 570				
A.D. 872 to A.D. 1012	570	T8-71	NW Tier M 35	1150	25
Mean = A.D. 946	580	T1-268	79	1185	20
	580	T1-232	60	Modern	
	590	8-58	NW Tier M 32	(–3580)	150
	590	T8-106	SE Tier M 30	1280	35
Event 7	Top of 600				
A.D. 731 to A.D. 856	600	T8-88	NW Tier M 36	1205	20
Mean = A.D. 796	600	T9-137	NW Tier 2 33-34	1600	20
	600	T9-140	NW Tier 2 33-34	(–4030)	100
	600	T1-254	68	1470	30
	620	8-72	SE Tier M 28	1280	25
	640 to 680	8-62	SE Tier L 31	1580	25
	640	T9-133	NW Tier 2 33-34	1620	40
	650 to 680	8-108	SE Tier M 18	1435	25
	650 to 680	8-107	SE Tier M 18	1260	25
	690	8-90	NW Tier M 11	Dissolved in pretreatment	
	690	8-37	SE Tier M 29	1520	25
	690	8-100	SE Tier L 12	1550	25
	670	T9-138	NW Tier 2 33-34	1980	30
	690	T9-139	NW Tier 2 33-34	1545	15
	690	T1-230	55	1550	20
	690	T8-93	NW Tier M 31	1720	20
	695	T8-89	NW Tier M 32	1505	20
Event 8	Top of 700				
A.D. 650 to A.D. 733	700	T8-76	SE Tier M 31	1365	20
Mean = A.D. 686	700	T1-234	60	1685	25
	700	T1-235	62	1725	20
	700	T9-97	NW Tier 2 31-32	2720	150
	710	T8-68	SE Tier M 28	1460	20
	710	8-47	SE Tier M 29	1910	25
	730	8-95	NW Tier M 31	Dissolved in pretreatment	
	750	8-28	NW Tier M 31	Dissolved in pretreatment	
	750	T8-79	SE Tier M 32	1995	20
	750	T1-239	63	(–1105)	35
	760	8-74	NW Tier M 11	1500	30
	790	8-96	NW Tier M 28	1575	25
	790	T9-135	NW Tier 3 32-34	1910	40
	790	T9-94	NW Tier 3 32-34	1725	30
	790	T8-191	SE Tier L 32	2390	60
	790	T8-153	SE Tier L 31	2040	40

(*continued*)

TABLE 1. RADIOCARBON DATES (*continued*)

Events	Unit	Sample no.	Trench panel*	^{14}C age (yr B.P.)	±1σ
Event 9	Top of 800				
A.D. 562 to A.D. 601 Mean = A.D. 582	800	T1-250	67	1705	25
	800	T8-800s	Seed from bulk sample	1500	15
	810	T8-810s	Seed from bulk sample	1510	20
	820	T9-30	SE Tier 2 22-23	1445	15
	850	T9-96	NW Tier 4 33-34	1640	15
	850	T8-187	SE Tier M 29	1580	20
	880	T9-35	SE Tier 4 31-32	3320	70
	890	T8-128	NW Tier M 11	1755	20
Event 10	Top of 900				
A.D. 300 to A.D. 387 Mean = A.D. 358	910	T9-70	SE Tier 4 33-34	1705	15
	910	8-123	NW Tier M 7	1705	25
	920	8-163	NW Tier L 11	1685	30
	940	8-181	NW Tier L 11	Dissolved in pretreatment	
	940	T9-60	NW Tier 4 32-33	1880	15
	940	T9-88	SE Tier 4 32-33	1805	15
	950	T8-141	SE Tier L 12	1720	20
	960	T9-93	SE Tier 4 31-32	1830	90
	960	T8-140	SE Tier L 12	2150	60
Event 11	Top of 970				
A.D. 235 to A.D. 328 Mean = A.D. 271	970	T8-133	SE Tier L 13	1835	35
	970	T8-134	SE Tier L 13	1770	20
	990	T8-116	NW Tier L 10	1780	20
	990	T9-108	NW Tier 4 32-33	1850	15
Event 12a, 12b	Top of 1000				
A.D. 147 to A.D. 216 Mean = A.D. 182	1000c	T9-90	SE Tier 4 32-33	1815	15
	1000	T8-1000ch	Charcoal from bulk sample	2100	15
	1020	T9-55	NW Tier 4 30-31	2210	15
	1020w	T9-82	SE Tier 4 32-33	1875	20
	1020	T9-117	SE Tier 4 26-27	1815	15
	1055w	T9-73	SE Tier 4 31-32	1925	20
Event 13	Top of 1060				
297 B.C. to A.D. 85 Mean = 102 B.C.	1060	T9-66	NW Tier 4 31-32	2210	15
	1060	T9-72	SE Tier 4 30-31	2480	15
	1060	T9-14	NW Tier 4 14-15	2885	20
Event 14	Top of 1070				
1275 B.C. to 1016 B.C. Mean = 1132 B.C.	1080	T9-126	NW Tier 4 11-12	3380	15
	1082	T9-26	SE Tier 4 12-13	3150	15
	1090	T8-121	NW Tier L 6	2920	70
	1090	T9-10	SE Tier 4 15-16	3090	20
	1090	T9-129	NW Tier 4 13-14	3130	15
	1095	T9-37	NW Tier 4 13-14	3320	20
Event 15	Top of 1150, Below 1090				
1581 B.C. to 1522 B.C. Mean = 1551 B.C.	1150	T9-20	NW Tier 4 11-12	3810	60
	1150	T9-78	NW Tier 4 11-12	3310	20
	1190	T9-19	NW Tier 4 11-12	3310	15
Event 16	Top of 1200				
1616 B.C. to 1556 B.C. Mean = 1587 B.C.	1200	T9-24	SE Tier 4 10-11	3290	15
	1200	T9-12	NW Tier 4 9-10	3525	20
	1200	T9-29	NW Tier 4 11-12	4040	60

Notes: Radiocarbon dates are presented in stratigraphic order, with event horizons denoted by underlined text. Gray shading indicates samples that were not used in the preferred OxCal model. Most of the shaded samples were eliminated because they were older than samples stratigraphically below them, or they were significantly older than samples within the same unit. Note, however, that some samples with older ages than those below them were retained when the probability distribution of the older and younger sample ages overlapped, such that the samples could be the same age or in time-stratigraphic order. Calibrated age ranges given for each event are 95.4% confidence intervals.

*Trench walls were divided into 1-m-wide panels on each trench tier, and panels were named according to their distance (in meter intervals) from a starting point at one end of each trench. Absolute locations of individual trench panels are not consistent between trenches.

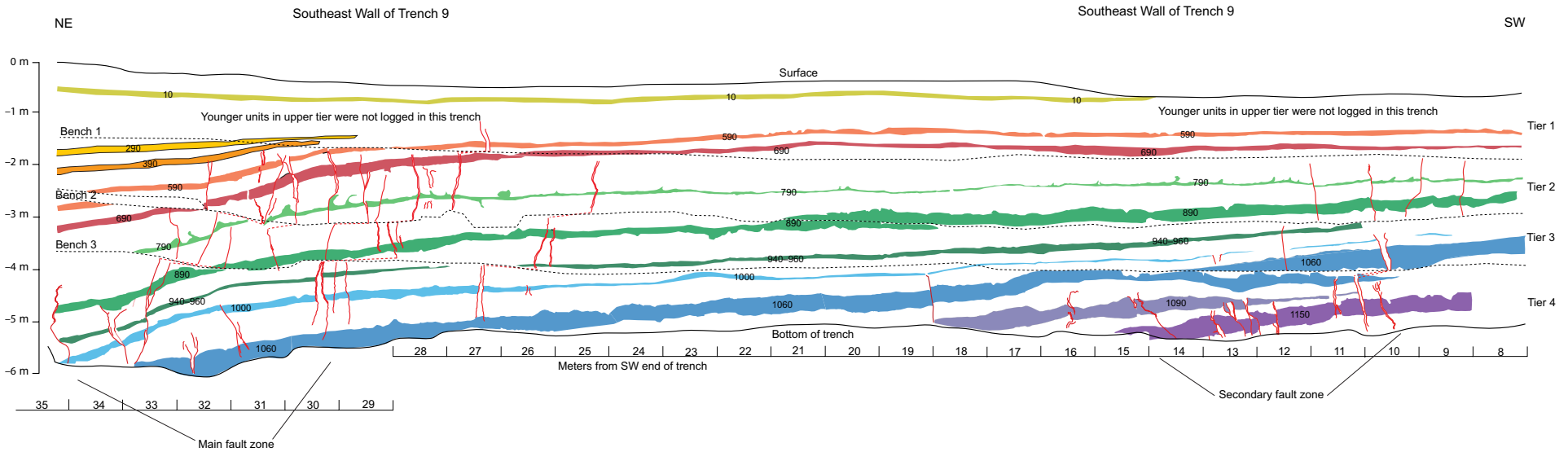

Figure 4. Stratigraphic marker units (colored layers) and faults (red lines) exposed in the southeast wall of trench 9. Note the folding and faulting concentrated on the main fault zone at the northeast end of the trench, with additional faulting in the secondary fault zone at the southwest end of the trench. Dashed lines mark the locations of the benches between tiered wall exposures. The apparent displacement of units across these benches is not real, but a result of the projection of multiple tier walls into a single plane for the figure.

RESULTS

The trenches exposed evidence for repeated surface ruptures along fault A (Fig. 2), which consisted of a main fault zone that showed northeast-side-down displacement, and a secondary fault zone 20 m to the southwest in the uplifted side (Fig. 4). Evidence of surface ruptures included upward terminations of faults, filled fissures, folding of strata across the main fault zone, and onlap of stratigraphic layers and angular unconformities associated with vertical movement across the main fault zone (Figs. 4–8). The earthquake record is most complete in the main fault zone at the northeast end of the trenches. There, the repeated subsidence of the sag during earthquakes creates accommodation space for additional sediment to be deposited, enabling us to distinguish between one earthquake rupture and the next. The stratigraphic level that represents the ground surface at the time of an earthquake and marks the upper limit of faulting at the site for that individual earthquake is defined as the "earthquake horizon." Almost all of the earthquake horizons at the Mystic Lake site occur at the top of fine-grained, dark, organic layers. We interpret these layers to be paleosols that developed at the surface during periods of depositional quiescence and soil formation in between earthquakes. On top of the earthquake horizons, there are lighter-colored clay or silty-clay deposits that are less tilted than the underlying organic-rich layers, and that thin as they approach and cross the main fault zone (Figs. 4–8). We interpret clay-rich layers to represent filling of the sag after it experienced subsidence during an earthquake. The stratigraphic relationships show that each successive rupture faulted and/or folded the soil that existed at the surface at the time of the earthquake, and then the sag slowly filled with sediment. A soil later developed at the surface on the new sediment until the next earthquake caused renewed subsidence.

We documented evidence for 16 surface ruptures over the past 3700 yr. Paleoseismic event evidence collected from the five trenches across fault A is shown in Figures 4 through 11 and summarized in Table 2. Evidence of the three oldest events (between 1700 B.C. and 1000 B.C.) was only found along fault strands within the secondary fault zone (Figs. 9–11), where older sediments have been elevated by southwest-side-up slip along the main fault zone of fault A. Trenches 8 and 9 were not deep enough to expose sediments of this age within the main fault zone, so we have no record of events between ~1000 B.C. and 100 B.C. (Fig. 12). We do believe we have a complete record, however, for the past 2000 yr, during which there were 12 or 13 ground-rupturing earthquakes. We generated probability density functions for the open intervals between each earthquake (we did not include the current open interval) and used the means of these individual distributions to estimate recurrence interval and the coefficient of variation. The mean recurrence time between earthquakes varied from 86 to 312 yr, with a mean recurrence interval for all 13 earthquakes of 160 yr and a standard deviation of 76. This results in a coefficient of variation of 0.48 for the past 2000 yr.

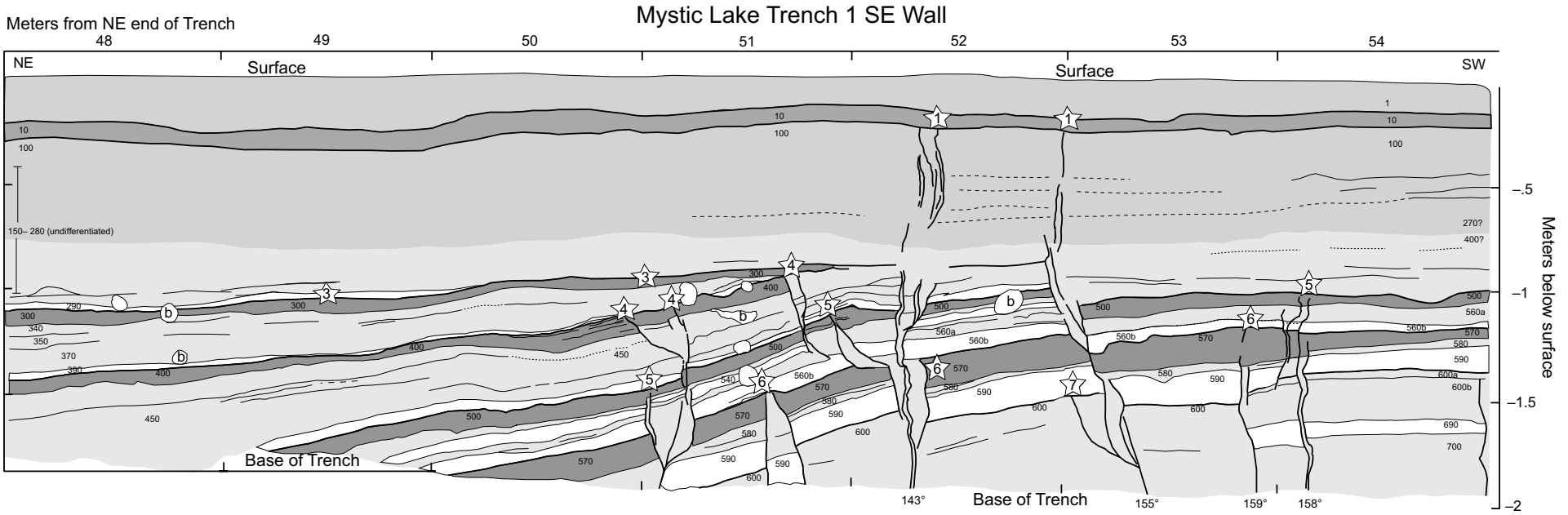

Figure 5. Stratigraphic and structural relationships exposed in the upper 1.5 m of trench 1 across the main fault zone of fault A (from Onderdonk et al., 2013). The photologs have been converted to artwork in this figure to highlight the stratigraphic relationships. Darker shaded units represent paleosol layers, white units represent clay-dominated layers, and lighter-gray units represent silt- or sand-dominated layers. Subvertical lines indicate faults, and white stars with numbers indicate respective earthquake horizons (location of the ground surface at the time of each earthquake). White "blobs" (some with the letter "b" in them) are burrows. Note the folding and thinning of layers across the fault zone, in addition to offsets and upward terminations of faults.

INTERPRETATIONS

Recurrence Intervals and the Current Open Interval

The Mystic Lake paleoseismic record (Fig. 12) shows no strong clustering of earthquakes during the past 2000 yr, and the 0.48 coefficient of variation suggests fairly regular ruptures. The most recent ground-rupturing earthquake occurred in the early 1800s. A rupture at the same time is also recorded at both of the two paleoseismic sites that have been studied farther to the northwest on the northern San Jacinto fault: the Quincy site (Onderdonk et al., 2015) and the Colton site (Kendrick and Fumal, 2005). This rupture may be one of two large historic earthquakes that caused damage at several Spanish missions in southern California on 22 November 1800 and 8 December 1812 (Toppozada et al., 2002). The 22 November 1800 earthquake, however, is interpreted to have occurred farther south along the San Jacinto fault, since it mainly caused damage at the San Juan Capistrano and San Diego missions, and it is preserved in paleoseismic records along the central San Jacinto fault (Salisbury et al., 2012; Rockwell et al., 2015). Grant Ludwig et al. (2015) hypothesized that the 8 December 1812 earthquake that ruptured the Mojave section of the San Andreas fault (Jacoby et al., 1988; Toppozada et al., 2002) also ruptured the San Jacinto fault, based on the low levels of ground motion required to preserve precariously balanced rocks in the area near the juncture of the two faults. Based on fitting dynamic rupture models to historic and paleoseismic records of this earthquake in the region, Lozos (2016) further hypothesized that this earthquake began on the northern San Jacinto fault and propagated onto the San Andreas fault. In light of these studies, we believe the most recent event at Mystic Lake was the 8 December 1812 earthquake. An alternative interpretation is that the most recent event on the northern San Jacinto fault was not substantial enough to be documented in historic records, but this seems unlikely because of the large size of the earthquake that should have occurred in a rupture that extended most of the length of the fault. The open interval that has occurred since the most recent earthquake is at least 167 yr, and possibly as long as 217 yr (206 yr if the earthquake occurred in A.D. 1812). This is equal to or longer than the average recurrence interval (160 ± 76 yr) for the northern San Jacinto fault during the past 2000 yr (Fig. 12), suggesting the fault may be near failure. There are three intervals between earthquakes, however, that may have been just as long, or longer, as the current open interval, given the uncertainties in earthquake ages. For example, the open interval between events 5 and 6 could have been as long as 400 yr if event 6 occurred at the oldest end of its possible time range and event 5 occurred at the young end of its time

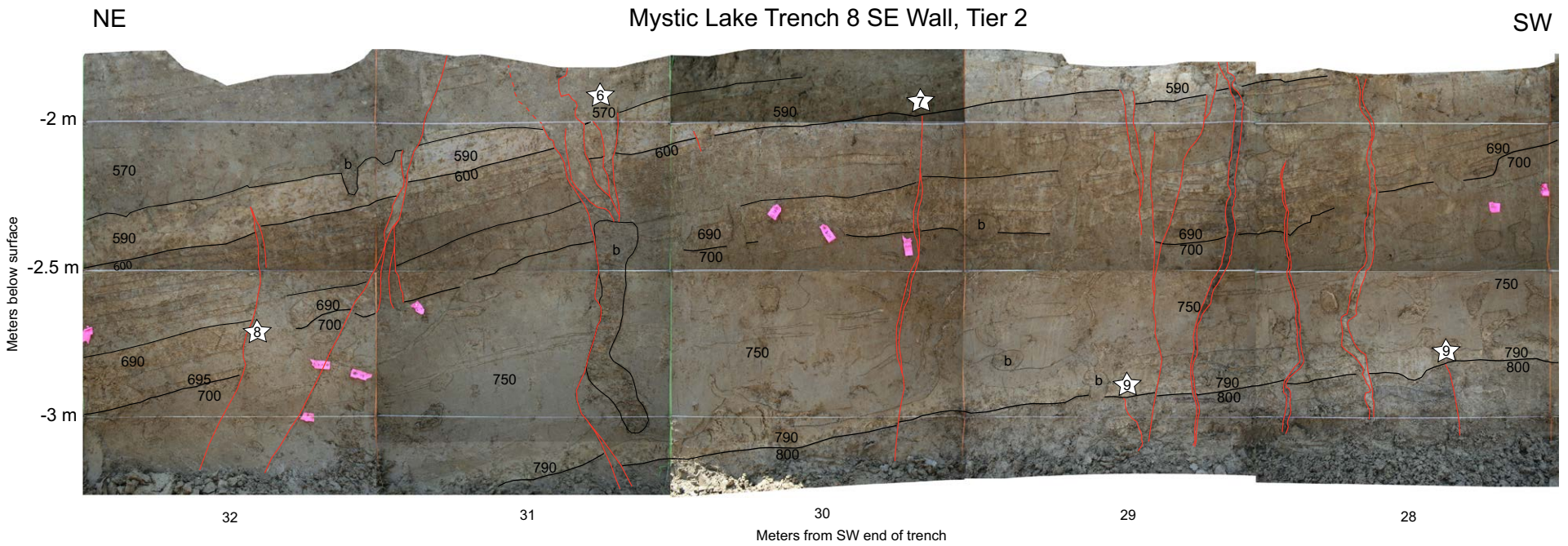

Figure 6. Evidence for events 6, 7, 8, and 9 in the main fault zone exposed in trench 8. Stratigraphic marker units (black lines) and faults (red lines) are plotted on images of tier 2 (of three tiers) of the southeast wall. Symbols/labels used in trench wall shown in Figures 6 through 11: black lines represent unit boundaries, with the slightly bolder lines denoting event horizons; darker units present below these event horizons are organic-rich layers interpreted to be paleosols, and the lighter units above the horizons are clay-dominated layers. Subvertical red lines indicate faults, and white stars with numbers indicate locations of evidence for specific earthquakes. White areas between images represent areas of no exposure due to benches between tiers, and the red dashed lines represent the extension of faults across the benches. Some larger burrows or bioturbation features are noted with the letter "b." Small pink, blue, and white flags and markers on the trench walls were used in the field to mark the locations of radiocarbon samples or other features.

range. Open intervals between events 6 and 7, and between events 9 and 10 could have been as long as 250 and 300 yr, respectively.

Similar relationships exist between the average recurrence interval and the present open interval for sites on the southern San Andreas fault (Fig. 13). At the Wrightwood paleoseismic site, on the Mojave section of the San Andreas fault, the most recent earthquake was in A.D. 1857 (160 yr ago), but the recurrence interval for the past 2000 yr is only 95 ± 5 yr (Scharer et al., 2010; Field et al., 2013). On the San Bernardino section of the San Andreas fault, the most recent earthquake was in A.D. 1812 (206 yr ago), while the recurrence interval is only 147 ± 14 yr at the Pitman Canyon site, and 173 ± 8 yr at the Burro Flats site (Field et al., 2013). However, like the Mystic Lake record, each one of these sites has open intervals in their prehistoric records that may be equally as long as the current open interval, given the uncertainties in event ages. The same is true when looking at the San Jacinto and San Andreas faults combined; there appears to be an unusual lack of ruptures in the area during the past 150 yr, but there are multiple time spans in the past 1200 yr where 150 yr intervals with no earthquakes on either fault are possible within the limits of dating uncertainties (for example, A.D. 900 to A.D. 1050, A.D. 1080 to A.D. 1240, or A.D. 1520 to A.D. 1680). Therefore, it appears that the current open interval may not be unusual and does not indicate some fundamental change in the fault system behavior.

Rupture across Stepovers

The northern San Jacinto fault (Claremont strand) forms a 2-km-wide stepover with the central San Jacinto fault (Clark strand), with ~24 km of overlap between the two faults (Fig. 1). The Mystic Lake site is located on the northern San Jacinto fault at the north end of this stepover, making it a good location at which to evaluate the possibility of rupture across the step. Both the Mystic Lake site on the northern San Jacinto fault and the Hog Lake site on the central San Jacinto fault (Rockwell et al., 2015) record at least 12 surface ruptures in the past 2000 yr (Fig. 13), but visual comparison of the two records shows no clear patterns of coincidence between ruptures on the two fault strands.

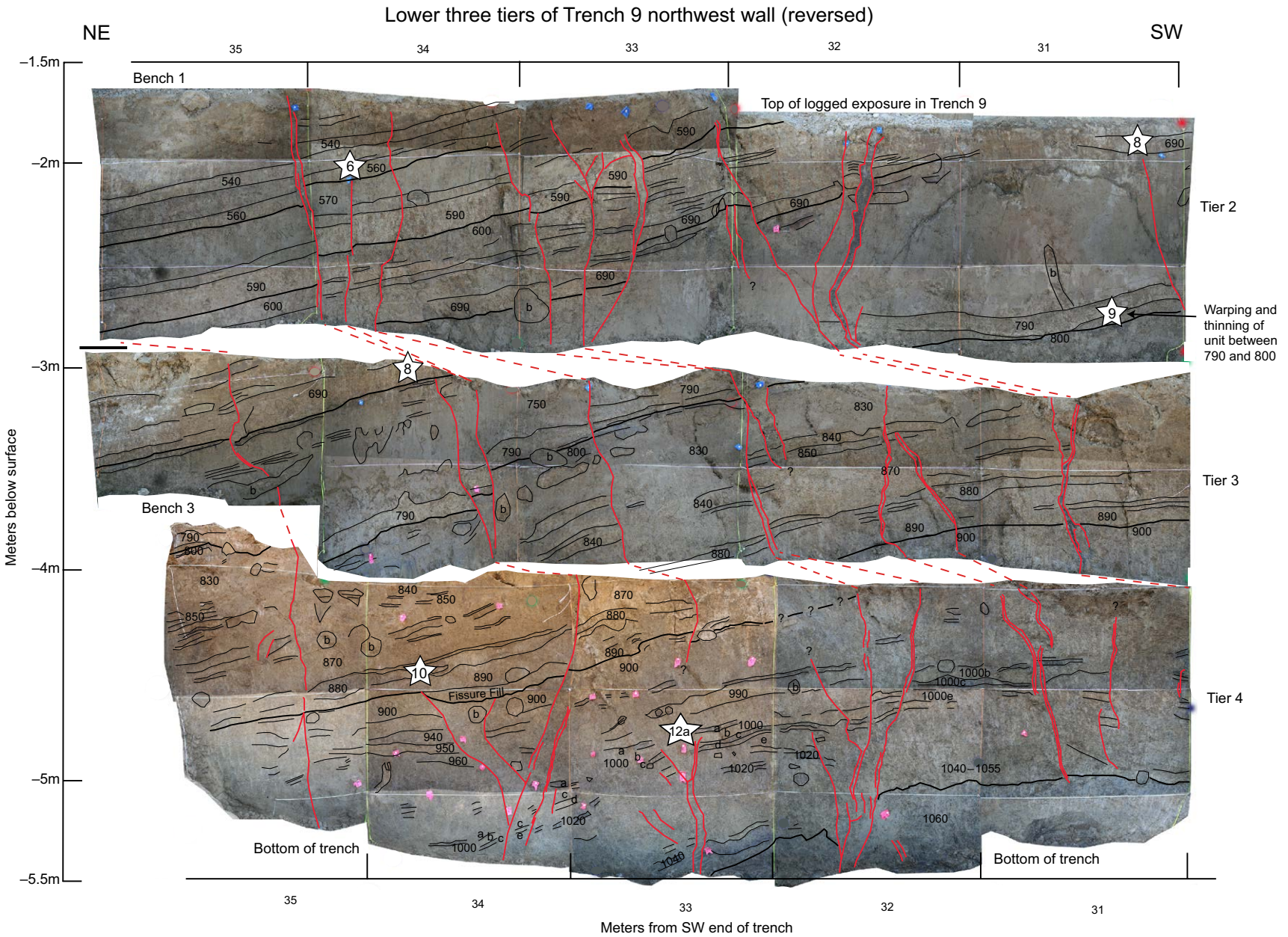

Figure 7. Examples of earthquake evidence for events 6, 8, 9, 10, and 12a from the northwest wall of trench 9 between 1.5 m and 5.5 m depth below the ground surface within the main fault zone of fault A. Note that this figure is a mirrored view (Fig. 8 is the opposite side). Refer to Figure 6 caption for explanation of symbols and labels.

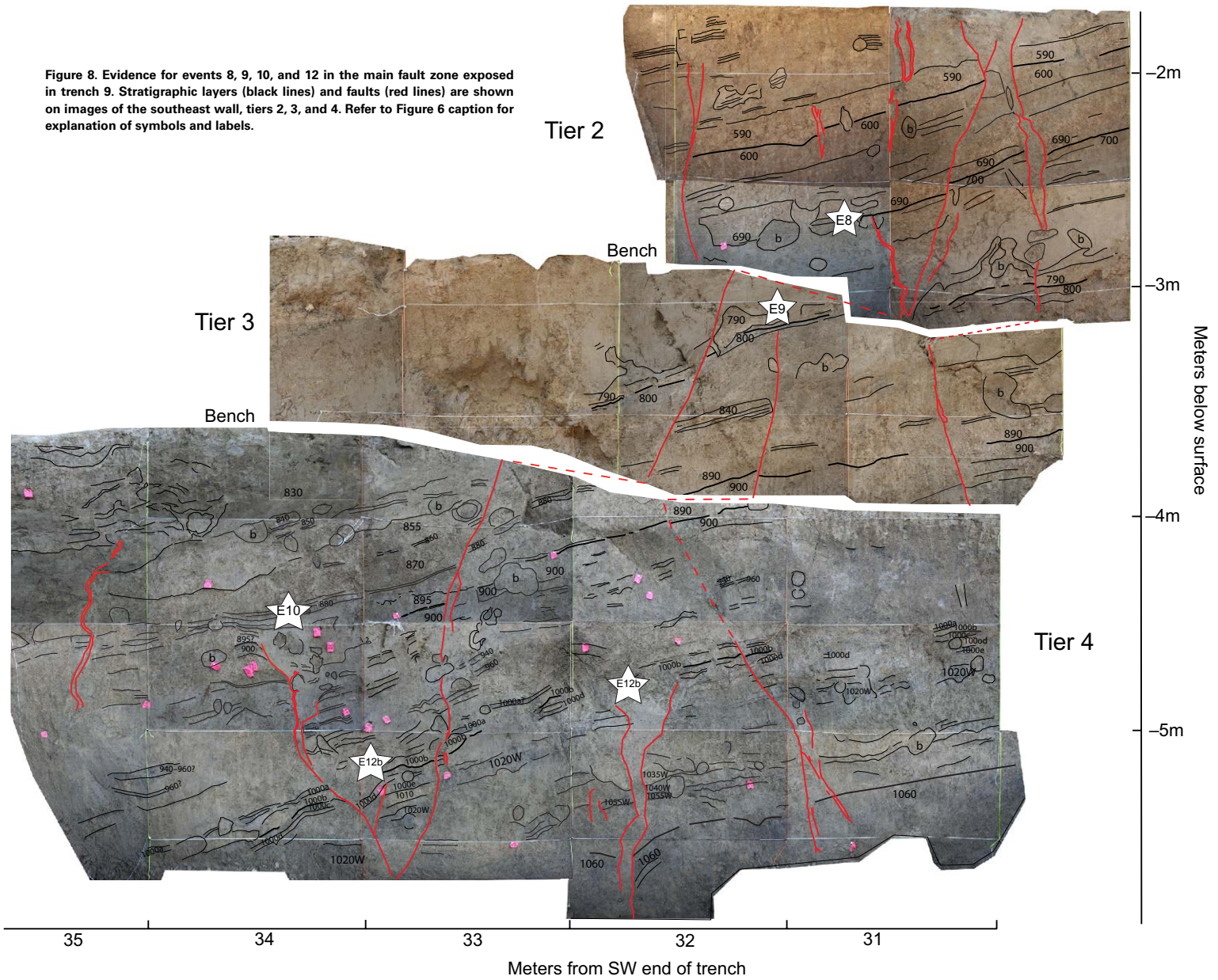

Figure 8. Evidence for events 8, 9, 10, and 12 in the main fault zone exposed in trench 9. Stratigraphic layers (black lines) and faults (red lines) are shown on images of the southeast wall, tiers 2, 3, and 4. Refer to Figure 6 caption for explanation of symbols and labels.

TABLE 2. EVENT EVIDENCE FROM MYSTIC LAKE TRENCHES

Event	Event horizon with respect to numbered units	Exposure: Trench no. (T) and meter no. (M) along the trench wall	Evidence	Confidence
ML0*	Top of 10 and possibly higher	T1 M52	Thickening of the sand layer across the fracture zone into the sag and folding of Unit 10 (Fig. 5)	Strong
		T7 M13	Faults offset Unit 10 with 1–3 cm down-to-the-northeast separation and may extend up into Unit 1 Upward termination of fractures Thickening of the sand layer across the fracture zone into the sag (see Onderdonk et al., 2013)	Strong
		T6 M17	Faults offset Unit 10 with down-to-the-SW displacement (see Onderdonk et al., 2013)	Strong
ML1	Top of 100	T1 M52,53	Upward termination of two clay seams with down-to-the-SW displacement (Fig. 5)	Strong
		T1 M17, 33	Faults cut Unit 200 and are lost in Unit 100 (see Onderdonk et al., 2013)	Weak
		T1 M76	Upward termination of fault	Strong
		T6 M14, 15 nwM13, 15	Upward termination of faults with down-to-the-NE displacement (see Onderdonk et al., 2013)	Strong
		T7 M13, 14, 15	Upward termination of numerous fractures without resolvable displacement and one or two faults that appear to disrupt two white silt layers within Units 100-200 (see Onderdonk et al., 2013)	Moderate
ML2	Top of 200	T1 M59 east	Upward termination of a fault, fissure fill	Strong
		T1 M18	Upward termination of a fault, SW side down (see Onderdonk et al., 2013)	Strong
		T1 M72	Upward termination of faults	Strong
		T1 M77	Upward termination of a fault	Strong
		T6 nwM16,17	Upward termination of faults (see Onderdonk et al., 2013)	Strong
ML3	Top of 300	T1 M33	Upward termination of faults, NE side down (Fig. 5)	Strong
		T1 M45-53	Folding of Unit 300 and below across the SW fault zone (Fig. 5)	Strong
		T7 M12	Upward termination of faults that define a graben	Strong
		T7 M7-12	Folding of Unit 300 and below, truncated by an angular unconformity at the base of Unit 250; onlap and pinching of Units 290, 270 against a fold scarp (see Onderdonk et al., 2013)	Strong
ML4	Top of 400	T1 M50,51	Upward termination of faults (Fig. 5)	Strong
		T1 M45-51	Thinning and pinching of Units 300–400 against the E4 fold scarp (Fig. 5)	Strong
		T6 M14	Upward termination of faults (see Onderdonk et al., 2013)	Strong
ML5	Top of 500	T1 M51	Upward termination of faults (Fig. 5)	Strong
		T1 M45-54	Thinning of units above the event horizon across the faults (Fig. 5)	Strong
		T6 M14	Upward termination of fault (see Onderdonk et al., 2013)	Strong
		T6 M16, 17	Possible upward termination of faults (see Onderdonk et al., 2013)	
ML6	Top of 570	T1 M51,52,53	Upward termination of faults (Fig. 5)	Strong
		T1 M53	Possible fissure fill (Fig. 5)	Weak
		T6 M14	Warping of strata against the fault (see Onderdonk et al., 2013)	Strong
		T6 M18	Upward termination of faults (see Onderdonk et al., 2013)	Strong
		T7 M31SE Tier 2, and M30-31 SE Tier 1	Unit 590 is offset, forming a graben that extends down into Unit 750; Unit 570 is filling the graben; Unit 560 is not offset, but it is discontinuous across the top due to bioturbation; Unit 560 is inferred to be unfaulted (see Onderdonk et al., 2013)	Moderate
		T9 M34 NW Tier 2	Fault cuts Unit 570 and below (down 8 cm on NE side) but does not cut the base of Unit 560 (Fig. 7)	Weak
		T8 M31 SE Tier 2	Fissure fill at the base of Unit 570 (Fig. 6)	Strong
ML7	Top of 600	T1 M53	Upward termination of fault (Fig. 5)	Strong
		T1 M54	Upward termination of fault (Fig. 5)	Strong
		T1 M73	Upward termination of faults (not shown)	Strong
		T8 M30 SE Tier 2	Units 690 and below are offset 2 cm down on the NE, but Unit 590 does not look offset (Fig. 6)	Moderate
ML8	Top of 700	T8 M32 SE Tier 2	Unit 690 thickens across a fault from 8–10 cm on the SW to about 20 cm on the NE with an intervening sand layer that probably came off the scarp; the Unit 690/700 contact is offset about 25 cm down on the NE side, while the upper contact of Unit 690 is only offset about 10 cm (by a later event that goes up through Unit 590 and offsets units between 690 and 590 by about 5 to 7 cm) (Fig. 6)	Strong

*ML0 is interpreted to be the result of local subsidence due to groundwater withdrawal in the twentieth century, and it was therefore not included as an earthquake in our event history (see Onderdonk et al., 2013).

(*continued*)

TABLE 2. EVENT EVIDENCE FROM MYSTIC LAKE TRENCHES (*continued*)

Event	Event horizon with respect to numbered units	Exposure: Trench no. (T) and meter no. (M) along the trench wall	Evidence	Confidence
ML8 (*continued*)		T8 M32 NW Tier 2	Unit 690 thickens across a fault that offsets Unit 790 about 3 to 4 cm down on the NE side; an adjacent fault offsets the base of Unit 690 about 10 cm, while the top of Unit 690 is only offset about 5 to 6 cm; a third fault cuts or warps Unit 700, but Unit 690 does not look offset (not shown in figures)	Strong
		T9 M31 NW Tier 2	Fault cuts Unit 790 and below, hard to trace through 700s but does not cut Unit 690 (Fig. 7)	Strong
		T9 M34 NW Tier 3	Fault cuts Unit 750 and below, but does not cut Unit 690 (Fig. 7)	Weak (could merge with adjacent fault)
ML9	Top of 800	T8 M29 SE Tier 2	Clay seam that offsets deeper layers is truncated at the base of Unit 790 (Fig. 6)	Strong
		T8 M28 SE Tier 2	Fault that offsets deeper layers is truncated at the base of Unit 790 (Fig. 6)	Strong
		T8 M13 SE Tier 2	Fault offsets Units 820, 840 and below (3 cm down-to-the-NE), but it is truncated at the base of Unit 790 (Fig. 6)	Strong
		T8 M32 SE Tier 3	Fault offsets Unit 800 and below down 4 cm on the NE side, but it does not cut Unit 790; Unit 790 thickens across the fault (not shown in figures)	Strong
		T9 M27 SE Tier 2	Fissure fill; Unit 790 dropping into a fissure in Unit 800, which is offset 5 cm on NE side (Fig. 8)	Strong
		T9 M32 SE Tier 3	Offset units below Unit 800 (up on NE side), but units 790 and 800 do not look offset (Fig. 8)	Weak (faults cannot be followed downward)
		T9 NW wall Tiers 2 and 3	Warping and pinching of fine-grained layer between Units 790 and 800 (Fig. 7)	Moderate
ML10	Top of 900	T8 M10 NW Tier 2	A graben drops Unit 900 down, but Units 850 and 840 are not disturbed, and Unit 890 seems to go across the fault undisturbed as well (Fig. 9)	Weak
		T8 M12 NW Tier 2	Unit 900 sags down, while Unit 890 goes straight across (Fig. 9)	Strong
		T8 M11 NW Tier 2	Unit 900 is tilted down between two faults; the fault on the right is probably capped by Unit 890 and is definitely capped by Units 850 and 840; the fault on the left goes up higher through Unit 790 (Fig. 9)	Strong
		T8 M29 SE Tier 3	Unit 900 is offset by a fault, but Unit 890 drapes across, and Units 840, 850 go right across (not shown in figures)	Moderate
		T8 M26 NW Tier 3	Fissure developed in Unit 900 and below; Unit 890 fills the fissure and drapes across (not shown in figures)	Strong
		T9 M34 NW Tier 4	Fissure cuts Unit 900 and below (down 10 cm on SW side), filled by Unit 880, which drapes across (Fig. 7)	Strong
		T9 M33 SE Tier 4	Fissure cuts Unit 900 and below (down 10 cm on SW side), filled by Unit 880, which drapes across (Fig. 8)	Strong
ML11	Top of 970	T8 M10 NW Tier 3	Faults cut and tilt Unit 990 and below, but do not cut Unit 960 (Fig. 9)	Strong
		T8 M11 NW Tier3	Faults cut and tilt Unit 990 and below, but do not cut Unit 960 (Fig. 9)	Strong
		T8 M12 NW Tier 3	Faults cut and tilt Unit 990 and below, and truncate Unit 970, but do not cut Unit 960 (Fig. 9)	Strong
ML12a	Top of 1000b	T9 M33 NW Tier 4	Fissure that may end upward around Unit 1000a or 1000b (clay that also fills the fissure?), and definitely ends below Unit 990 (Fig. 7)	Moderate
ML12b	Top of 1000c	T9 M33 SE Tier 4	A fault offsets Unit 1020, truncates Units 1010 and 1000e, and sharply warps Units 1000d (sand) and 1000c (dark layer); Unit 1000b (clay) thickens across the scarp, thus postdating the event (Fig. 8)	Moderate
		T9 M32 SE Tier 4	Fissure that is capped around Unit 1000b (Fig. 8)	Weak
ML13	Top of 1060	T9 Whole trench	Units between 1060 and 1020 pinch out against Unit 1060 from NE to SW; Unit 1060 is tilted more than units above; strong tilt at M16 and another strong warp (possibly offset) at M24 (Fig. 4)	Strong
ML14	Base of 1060 or within 1070	T9 M11-13 SE Tier 4	Unit 1082 offset 10 cm down to NE; base of Unit 1060 not cut; faults extend down into a graben at depth that does not affect Unit 1060 (Fig. 10)	Moderate
ML15	Base of 1090	T9 M14 NW Tier 4	Unit 1200 is offset 10 to 15 cm down-to-the-NE; fissures in Unit 1150, but base of 1090 is not cut	Strong
		T9 M12 NW Tier 4	Fractures cut up through Unit 1150, but do not cut Unit 1090 (Fig. 11)	Moderate
ML16	Base of 1150	T9 M14 NW Tier 4	Top of Unit 1200 is offset, but the top of Unit 1200 does not continue to the faults that define the next higher event (E15), suggesting that a fissure existed in Unit 1200 before Unit 1150 was deposited; also a thin clay layer (Unit 1190) drapes across the offset Unit 1200, and this clay layer is offset by E15 faults (Fig. 11)	Moderate

Notes: Summary of evidence for earthquakes on the primary active strand (fault A) at Mystic Lake, with reference to the figures that show evidence for each event. Event evidence from trenches T1, T8, T9 is shown in Figures 4–11. Note that not all event evidence is shown in the figures presented here; photologs of trenches T6 and T7 were presented in Onderdonk et al. (2013).

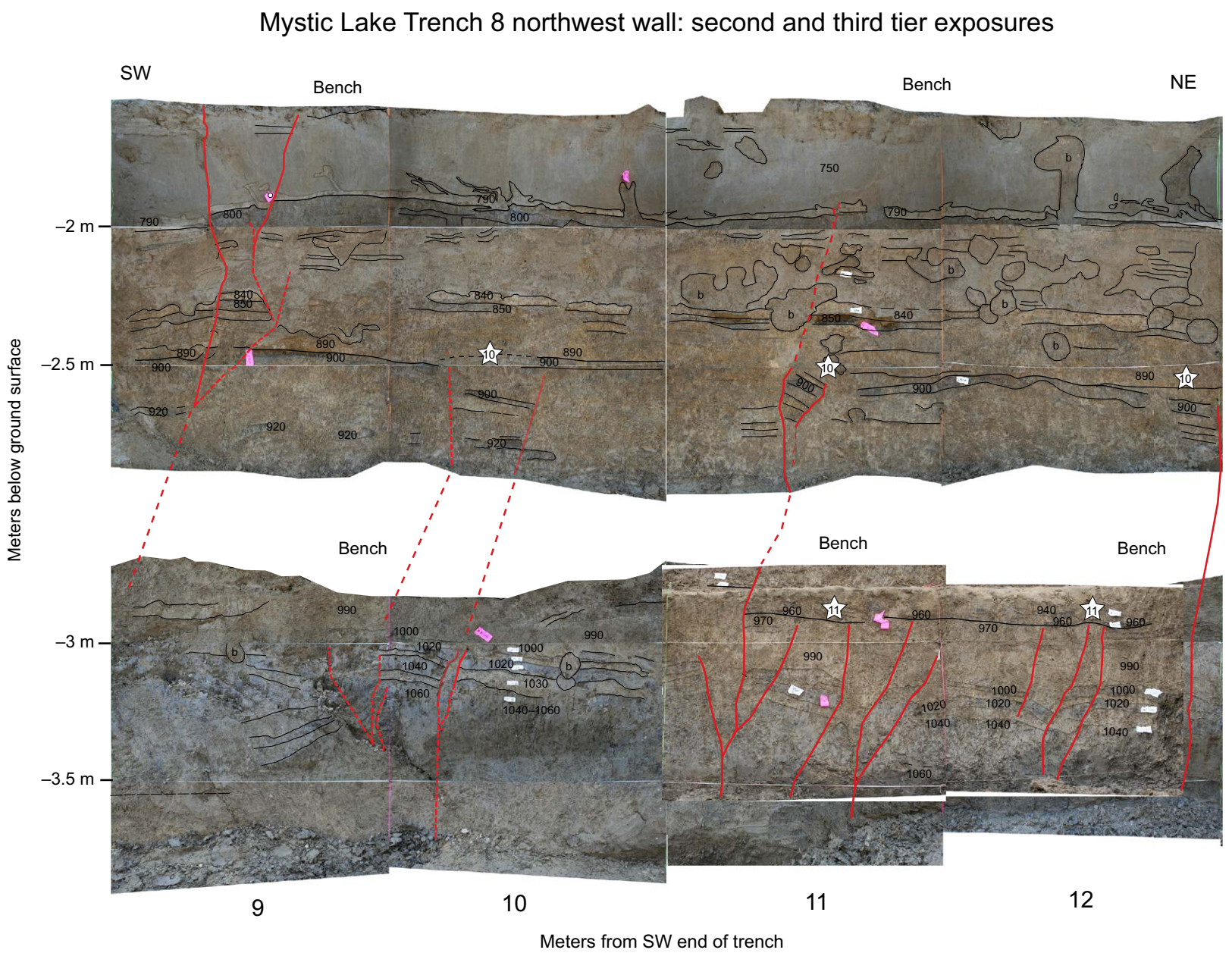

Figure 9. Evidence for events 10 and 11 in the secondary fault zone in trench 8. Stratigraphic marker units and faults are plotted on images of the middle and lower tiers of the northwest wall. Refer to Figure 6 caption for explanation of symbols and labels.

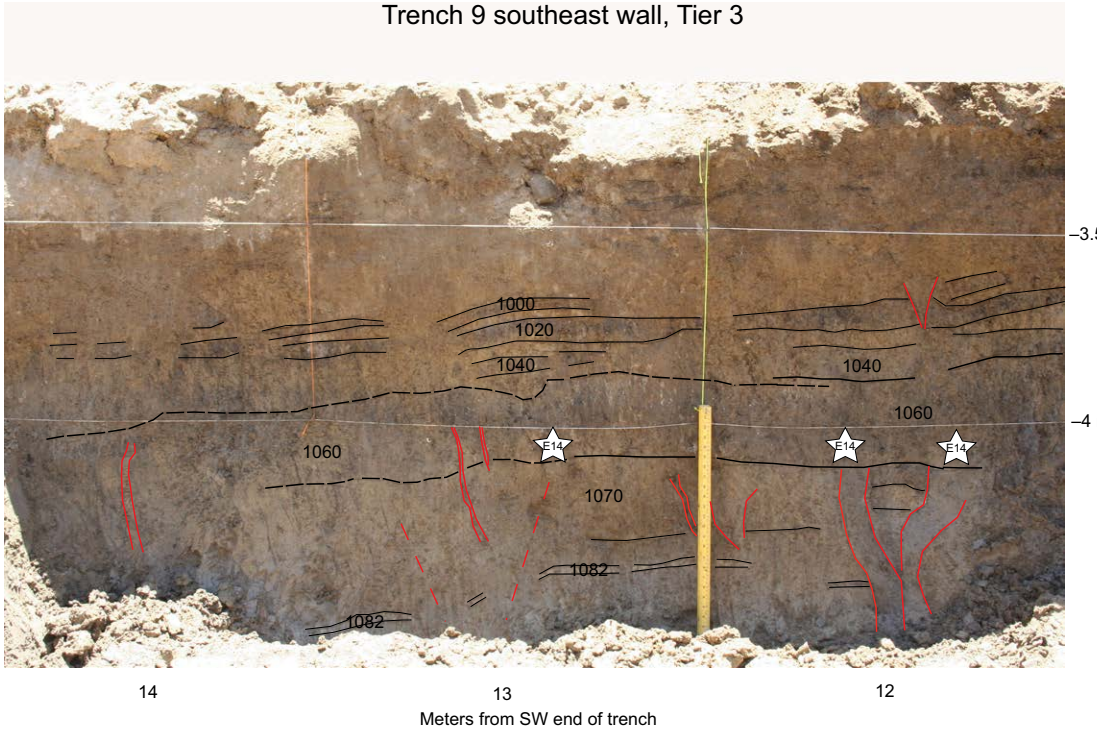

Figure 10. Evidence for event 14 in the secondary fault zone exposed in trench 9. Unit 1082 is offset ~10 cm down to northeast. Unit 1060 appears undisturbed and does not thicken across the zone in which unit 1082 is offset. Several clay-filled seams and fissures end at or within a few centimeters of the base of unit 1060, suggesting that the event occurred shortly prior to deposition of unit 1060. The fault zone that offsets unit 1082 continues downward into tier 4, where it is expressed as a graben. Refer to Figure 6 caption for explanation of symbols and labels.

Relative quiet on one fault strand during some time periods while the other is more active suggests these fault strands are not rupturing together or triggering each other most of the time. There are, however, three events for which the age ranges are almost identical at the two sites (ML3, ML6, and ML11), which tempts the interpretation that these events may have ruptured both fault strands. However, uncertainties in the event dates (typically tens to hundreds of years) make it impossible to correlate events from two different paleoseismic sites. Statistical analysis of overlapping probability density functions for earthquakes does not provide any benefit to correlation confidence, since even fully overlapping probability density functions only provide a range of time during which two completely unrelated earthquakes could have occurred decades or even years apart. For this reason, additional constraints, such as event size and/or rupture length, are needed to evaluate the probability of event correlation between two sites (e.g., Biasi and Weldon, 2009). For the rupture histories considered here, measurements of slip-per-earthquake on the northern San Jacinto fault provide information about the average earthquake size that supports the idea of occasional joint rupture of fault strands separated by steps at the north and south ends of the Claremont strand. The age of offset streams and timing of earthquakes at the Quincy site (Fig. 1) indicate that the average slip during ruptures in the past 11 or 12 earthquakes was 2.5 m, and greater than 3 m for the last three earthquakes (Onderdonk et al., 2015). If we assume that slip measurements at the site are representative of the average surface slip along the rupture length of these earthquakes, then the observed value of 2.5 m or more of slip in these events suggests rupture lengths of ~110 km or more (Wells and Coppersmith, 1994), which is longer than the 75 km total length of the Claremont strand. The earthquakes that were larger than the average, especially one or more of the last three, likely extended beyond the length of the fault and continued through one of the steps at either end of the Claremont strand. The strongest evidence for this exists for event 3 at Mystic Lake, which we interpret to have been a very large earthquake based on the large amount of tilting observed in the Mystic Lake trenches at the stratigraphic level of event 3, and evidence of 3.1 m to 3.6 m of lateral slip during this event at the Quincy site (Onderdonk et al., 2013, 2015).

Cajon Pass "Earthquake Router"

During the past 1000 yr, there were nine earthquakes recorded on the Mojave section of the San Andreas fault at Wrightwood, but only six recorded at paleoseismic sites on the San Bernardino section of the San Andreas fault

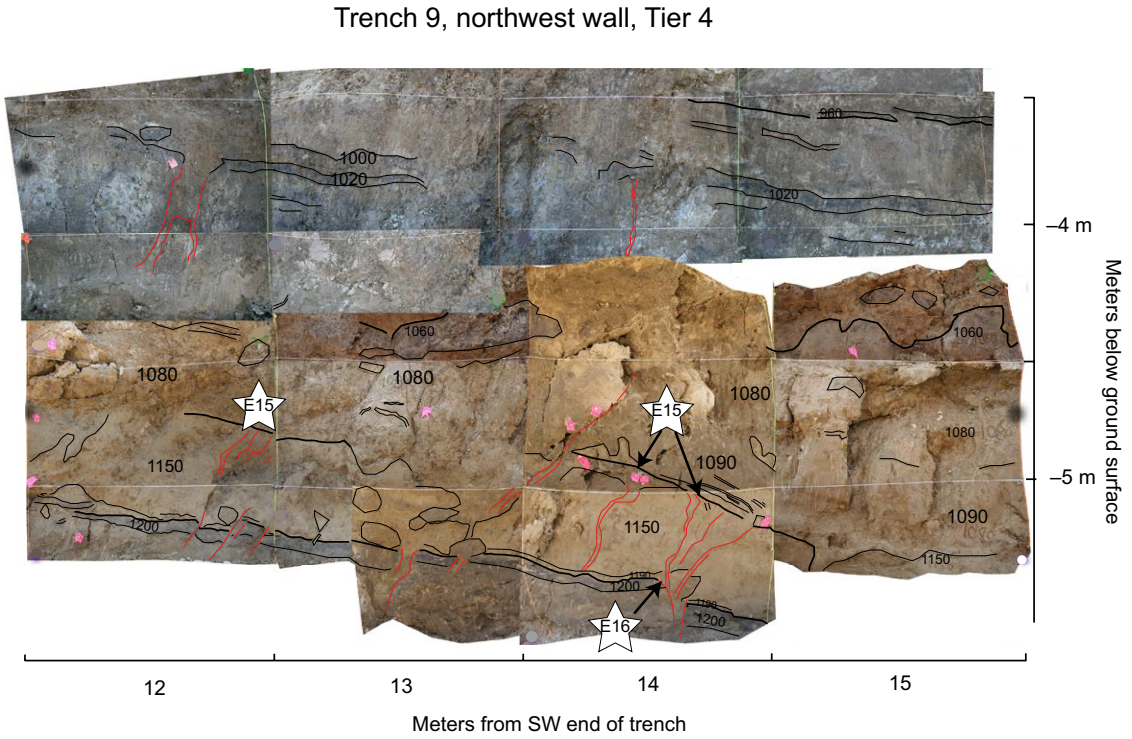

Figure 11. Evidence for events 15 and 16 in the secondary fault zone exposed in tier 4 of trench 9. Stratigraphic marker units and faults are plotted on images of the middle and lower tiers of the northwest wall. Refer to Figure 6 caption for explanation of symbols and labels.

to the southeast (Fig. 13). An additional nine earthquakes were recorded at Wrightwood during the preceding millennium, while only three are recorded in the record from Burro Flats. No data exist for this earlier time period from the Pitman Canyon site, but unless there was a big change in recurrence interval around A.D. 1000, we can assume that there were a larger number of earthquakes on the San Andreas fault northwest of Cajon Pass than to the southeast for the past 2000 yr. This suggests that some ruptures on the Mojave section of the San Andreas fault stop in Cajon Pass, as did the Fort Tejon earthquake in 1857, with Cajon Pass acting as an "earthquake gate" (term from Oskin et al., 2015), which can inhibit or facilitate a through-going rupture. However, the structure and tectonic geomorphology of the San Andreas fault through Cajon Pass are relatively continuous and show no obvious indication of a barrier to rupture propagation at the surface (e.g., Sedki, 2013; USGS Q-faults database: Machette et al., 2004) or in three-dimensional fault models (Plesch et al., 2007). If large ruptures on the Mojave segment of the San Andreas fault are occasionally starting or stopping in Cajon Pass, work is needed to identify the type of geologic, structural, or stress conditions that are responsible for this.

An alternative to ruptures stopping in Cajon Pass is the possibility of rupture being directed onto the adjacent San Jacinto fault, and several lines of evidence support this interpretation. First, the differences between the number of earthquakes recorded on the San Andreas fault north and south of Cajon Pass, and the recurrence intervals for the three fault sections show that the Mojave section of the San Andreas fault ruptures almost twice as frequently as the San Bernardino section of the San Andreas fault or the San Jacinto fault (Fig. 13). Second, the spatial distributions of slip rates on the San Andreas fault and San Jacinto fault indicate that displacement is being transferred between the two faults. The ~34 mm/yr slip rate of the Mojave section of the San Andreas fault (e.g., Dawson and Weldon, 2013) is divided between the San Bernardino section of the San Andreas fault (7–15.7 mm/yr; McGill et al., 2013) and the northern San Jacinto fault (12.8–18.3 mm/yr; Onderdonk et al., 2015), with 2–5 mm/yr possibly distributed to the reverse faults at the margins of the San Gabriel and San Bernardino Mountains (McGill et al., 2013, 2015). A correlative distribution of coseismic slip on the Mojave section of the San Andreas fault between these two fault sections to the southeast and south would be a simple way of accommodating the division of accumulated slip from the Mojave segment of the San Andreas fault southward. Third, the average slip-per-event on the northern San Jacinto fault indicates that some ruptures on the fault may have extended beyond one (or both) of the stepovers at the ends of the fault.

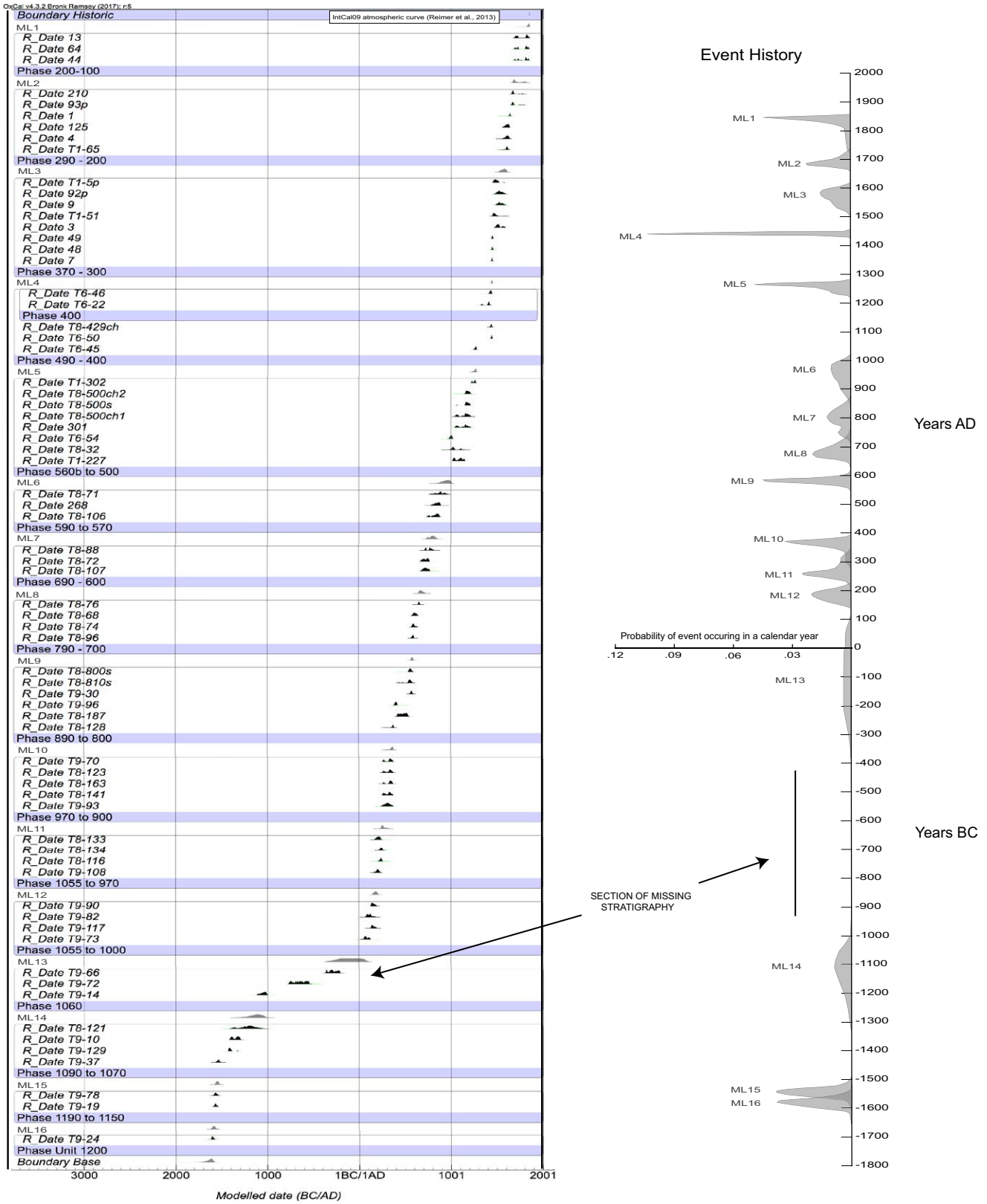

Figure 12. Left: Modeled ages of ^{14}C (R_Date "Sample number") dates and earthquake events (ML "event number") plotted in stratigraphic order. Black and gray shapes represent probability density functions of radiocarbon dates and earthquake ages, respectively. Right: Probability density functions of the event ages plotted in time.

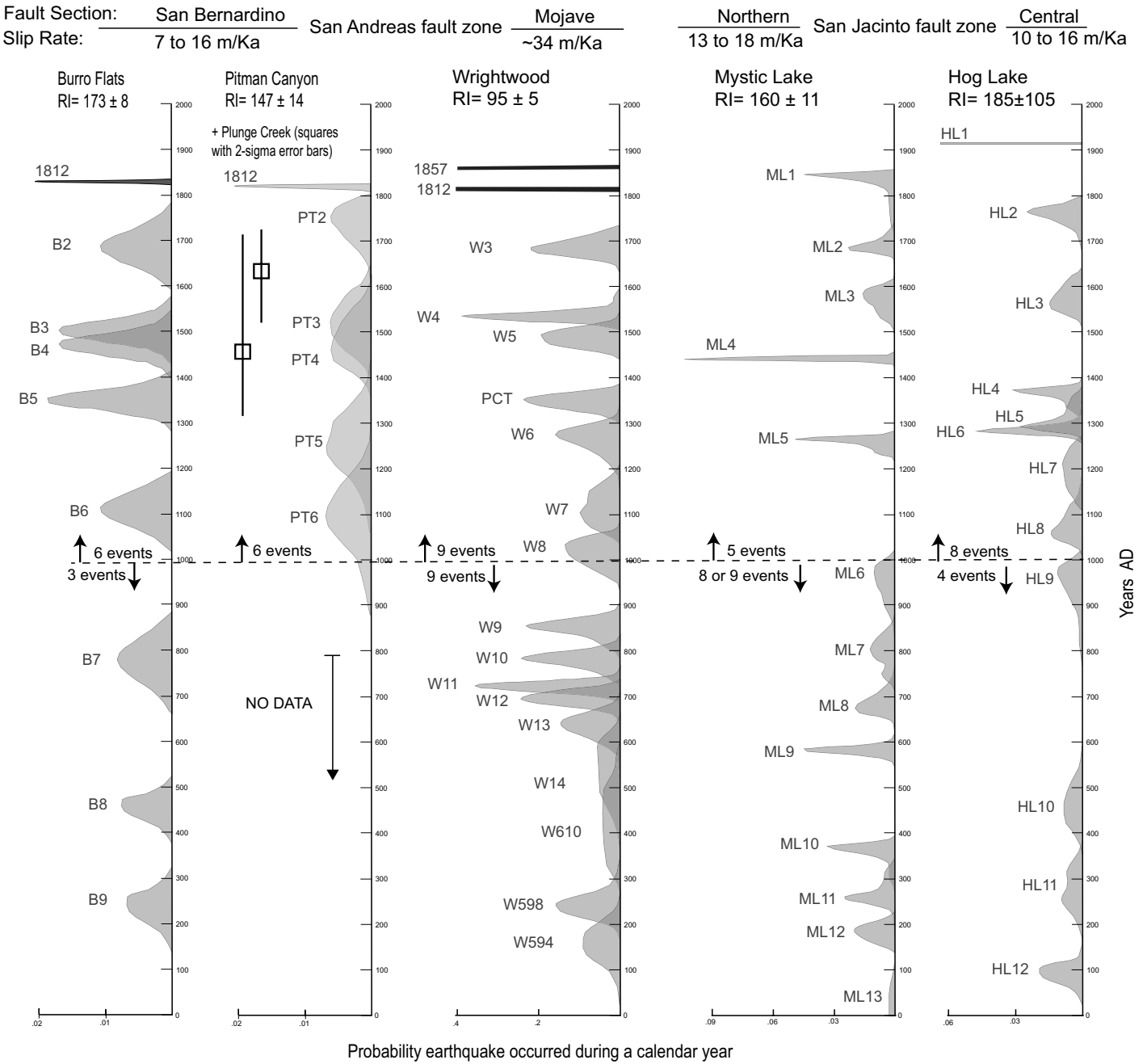

Figure 13. Probability density functions representing the timing of earthquakes for the past 2000 yr from paleoseismic sites on the San Andreas and San Jacinto faults near their juncture. The Wrightwood site (Fumal et al., 2002) is shown in the middle, the Mystic Lake site (this study) and the Hog Lake site (Rockwell et al., 2015) on the San Jacinto fault are shown to the right, and the Pitman Canyon (Seitz et al., 1997), Plunge Creek (McGill et al., 2002), and Burro Flats (Yule and Sieh, 2001) sites on the San Andreas fault south of the San Andreas–San Jacinto juncture are on the left. Event histories from the San Andreas sites are updated event ages from Field et al. (2013). RI—recurrence interval. Individual event PDFs for each paleoseismic site are labeled with a letter representing the site name, and a number representing the chronological order of the events at each site.

The stepover between the northern end of the San Jacinto fault and the San Andreas fault in Cajon Pass is only 1.6 km wide (Fig. 1), which is narrow enough to allow rupture propagation between the two faults, based on observations of historic ruptures across stepovers (Wesnousky, 2006). These characteristics of the three fault sections lead us to infer that some of the San Andreas fault ruptures that are "missing" from the San Bernardino segment of the San Andreas fault paleoseismic sites are present in the Mystic Lake record and represent joint rupture of the Mojave segment of the San Andreas fault and the northern San Jacinto fault. We note that if the Burro Flats paleoseismic record is complete (or mostly complete) for the past 2000 yr, then joint rupture of the San Andreas fault and San Jacinto fault may have been more common between A.D. 0 and A.D. 1000 than during the past 1000 yr. Activity at the Wrightwood site has been relatively constant during the past 2000 yr, with nine earthquakes recorded in each of the past two millennia (Fig. 13). However, the San Bernardino section of the San Andreas fault appears to have been more active between A.D. 1000 and the present, with six earthquakes recorded at Burro Flats, compared to only three between A.D. 0 and A.D. 1000. The Mystic Lake site shows an opposite pattern, with five earthquakes between A.D. 1000 and the present, compared to eight earthquakes between A.D. 0 and A.D. 1000.

These observations of San Jacinto fault and San Andreas fault kinematics support previous interpretations based on modeling and inferred strong ground motion patterns that inferred that ruptures can propagate from one fault to the other in the Cajon Pass area (Anderson et al., 2003; Grant Ludwig et al., 2015; Lozos, 2016). Grant Ludwig et al. (2015) also suggested that ruptures that did not jump across the step most likely started or stopped in Cajon Pass, and that through-going rupture on the San Andreas fault is rare. Our comparison of paleoseismic data from the past 2000 yr presented here cannot directly test the idea that through-going ruptures on the San Andreas fault are rare. However, the paleoseismic data do provide another line of evidence that supports the idea that the Cajon Pass area acts as an "earthquake router," where ruptures have an end point in the Cajon Pass area, propagate across the step from one fault to another (or to one of the reverse faults of the Transverse Ranges), or continue through on the San Andreas fault.

Implications for a Large Southern San Andreas Earthquake

The possibility of joint rupture of the northern San Jacinto fault and the Mojave segment of the San Andreas fault has implications for probabilities of major earthquakes in the southern California fault system. To explore the effects on the population of southern California, Jones et al. (2008) modeled a large rupture on the southern San Andreas fault, nucleating on the Coachella Valley section of the San Andreas fault and propagating northward through the San Gorgonio Pass onto the Mojave segment of the San Andreas fault (called "The ShakeOut Scenario"). We propose that a more likely scenario for such a large event is the joint rupture of the San Jacinto fault and the Mojave section of the San Andreas fault, because this scenario involves a rupture path that has less structural complexity than the southern San Andreas fault. The southern San Andreas fault includes a structurally complex restraining bend in the San Gorgonio Pass, composed of an oblique-thrust system with strike-slip tear faults that link the San Andreas fault in Coachella Valley to the San Bernardino area (e.g., Morton and Matti, 1993; Yule and Sieh, 2003). Conversely, the San Jacinto fault is straighter and contains only narrow dilational steps that modeling suggests are mechanically easier for ruptures to pass through than similar-sized restraining bends or steps (Oglesby, 2005). In a large southern San Andreas fault rupture (e.g., Bombay Beach to the Mojave segment of the San Andreas fault, as modeled by Jones et al., 2008), average displacement would be expected to be 4 m or more, and it is more likely to be near the maximum in the middle of the rupture along the San Bernardino segment. Average slip-per-event on the San Bernardino segment of the San Andreas fault during the past 1000 yr, calculated from the number of earthquakes at Pitman Canyon and Burro Flats and the latest Pleistocene slip rate (McGill et al., 2013), is only 1.2–2.7 m/event. This is not as high as would be expected if a full southern San Andreas fault rupture had occurred during this time period, and it is lower than the average slip-per-event values for the past 1000 yr on the northern San Jacinto fault (2.5–3.5 m/event: Onderdonk et al., 2015) and the Mojave segment of the San Andreas fault (3.9 m/event: calculated here from the number of earthquakes recorded at the Wrightwood site and the slip rate). This suggests a "ShakeOut Scenario" event has not occurred in the past 1000 yr. Heermance and Yule (2017) showed that the thrust system in the San Gorgonio Pass has experienced offsets of 4–8 m in single events that may involve the San Andreas fault on both sides of the pass, but they noted that these are infrequent events (once every 1000–1500 yr). The long intervals between ruptures in the San Gorgonio Pass area also indicate that some of the hypothesized correlations between earthquakes recorded at paleoseismic sites on the San Andreas fault in Coachella Valley and the San Bernardino area (e.g., Philibosian et al., 2011; Rockwell et al., 2016) are incorrect and that the "ShakeOut Scenario" is not as common as these correlations would suggest. This is supported by observations that precariously balanced rocks exist in the San Bernardino Mountains near the San Andreas fault, where strong ground motion would be expected from a large San Andreas fault rupture that extended from Coachella Valley through the Cajon Pass (Grant Ludwig et al., 2015). Such a rupture would have toppled the precariously balanced rocks, indicating that a large rupture on the San Andreas fault through this area has not occurred in several thousand years (Grant Ludwig et al., 2015). The available paleoseismic data, average slip-per-event data, distribution of precariously balanced rocks, and the structural geometry of the two fault zones summarized here suggest to us that very large earthquakes in the southern San Andreas fault system may be more likely to occur from joint rupture of the Mojave segment of the San Andreas fault and the San Jacinto fault, rather than a San Andreas fault–only rupture from the Mojave Desert to Coachella Valley.

ACKNOWLEDGMENTS

We thank the following former students and Southern California Earthquake Center (SCEC) interns for assistance in the field: Paul Alessio, Matt Cole, Ryan Danielson, Eric Gordon, Eric Haaker, Julian Lozos, Rainer Luptowitz, Gayatri Marliyani, Walter Nelson, Elizabeth Niespolo, Matthew Warbritton, and Neta Wechsler. We also thank Scott Sewell of the San Jacinto Wildlife Area for his assistance with this project and allowing us to access the Mystic Lake site. We thank Doug Yule, Glen Biasi, and three anonymous reviewers for their excellent reviews of earlier versions of this paper. This work was funded by U.S. Geological Survey (USGS) Earthquake Hazard Program grants (G11AP20136, G11AP20138, G11AP20142), and several grants from the SCEC. SCEC is funded by National Science Foundation Cooperative Agreement EAR-0106924 and USGS Cooperative Agreement 02HQAG0008. This is SCEC contribution 6238. The views and conclusions contained in this document are those of the authors and should not be interpreted as representing the opinions or policies of the U.S. Geological Survey. Mention of trade names or commercial products does not constitute their endorsement by the U.S. Geological Survey.

REFERENCES CITED

Anderson, G., Aagaard, B., and Hudnut, K., 2003, Fault interactions and large complex earthquakes in the Los Angeles area: Science, v. 302, p. 1946–1949, https://doi.org/10.1126/science.1090747.

Biasi, G., and Weldon, R., 2009, San Andreas fault rupture scenarios from multiple paleoseismic records: Stringing pearls: Bulletin of the Seismological Society of America, v. 99, p. 471–498, https://doi.org/10.1785/0120080287.

Blisniuk, K., Oskin, M., Meriaux, A., Rockwell, T., Finkel, R., and Ryerson, F., 2013, Stable, rapid rate of slip since inception of the San Jacinto fault, California: Quaternary San Jacinto fault slip rates: Geophysical Research Letters, v. 40, p. 4209–4213, https://doi.org/10.1002/grl.50819.

Bronk Ramsey, C., 2009, Bayesian analysis of radiocarbon dates: Radiocarbon, v. 51, p. 337–360, https://doi.org/10.1017/S0033822200033865.

Bronk Ramsey, C., 2017, Methods for Summarizing Radiocarbon Datasets: Radiocarbon, v. 59, p. 1809–1833, https://doi.org/10.1017/RDC.2017.108.

Dawson, T., and Weldon, R., 2013, Geologic-slip-rate data and geologic deformation model, Appendix B, *in* Field, E.H., Biasi, G.P., Bird, P., Dawson, T.E., Felzer, K.R., Jackson, D.D., Johnson, K.M., Jordan, T.H., Madden, C., Michael, A.J., Milner, K.R., Page, M.T., Parsons, T., Powers, P.M., Shaw, B.E., Thatcher, W.R., Weldon, R.J., II, and Zeng, Y., contributors, Uniform California Earthquake Rupture Forecast, Version 3 (UCERF3)—The Time-Independent Model: U.S. Geological Survey Open-File Report 2013–1165, California Geological Survey Special Report 228, and Southern California Earthquake Center Publication 1792, 97 p.

Field, E.H., Biasi, G.P., Bird, P., Dawson, T.E., Felzer, K.R., Jackson, D.D., Johnson, K.M., Jordan, T.H., Madden, C., Michael, A.J., Milner, K.R., Page, M.T., Parsons, T., Powers, P.M., Shaw, B.E., Thatcher, W.R., Weldon, R.J., II, and Zeng, Y., contributors, 2013, Uniform California Earthquake Rupture Forecast, Version 3 (UCERF3)—The Time-Independent Model: U.S. Geological Survey Open-File Report 2013–1165, 97 p., https://doi.org/10.3133/ofr20131165.

Fumal, T., Weldon, R., Biasi, G., Dawson, T., Seitz, G., Frost, W., and Schwartz, D., 2002, Evidence for large earthquakes on the San Andreas fault at Wrightwood, California, paleoseismic site: AD 500 to present: Bulletin of the Seismological Society of America, v. 92, p. 2726–2760, https://doi.org/10.1785/0120000608.

Grant Ludwig, L., Brune, J., Anooshehpoor, A., Purvance, M., Brune, R., and Lozos, J., 2015, Reconciling precariously balanced rocks (PBRs) with large earthquakes on the San Andreas fault system: Seismological Research Letters, v. 86, p. 1345–1353, https://doi.org/10.1785/0220140239.

Heermance, R., and Yule, D., 2017, Holocene slip rates along the San Andreas fault system in the San Gorgonio Pass and implications for large earthquakes in southern California: Geophysical Research Letters, v. 44, p. 5391–5400, https://doi.org/10.1002/2017GL072612.

Jacoby, G., Jr., Sheppard, P., and Sieh, K., 1988, Irregular recurrence of large earthquakes along the San Andreas fault: Evidence from trees: Science, v. 241, p. 196–199, https://doi.org/10.1126/science.241.4862.196.

Jones, L., Bernknopf, R., Cox, D., Goltz, J., Hudnut, K., Mileti, D., Perry, S., Ponti, D., Porter, K., Reichle, M., Seligson, H., Shoaf, K., Treiman, J., and Wein, A., 2008, The ShakeOut Scenario: U.S. Geological Survey Open-File Report 2008–1150, 312 p.

Kendrick, K.J., and Fumal, T., 2005, Paleoseismicity of the northern San Jacinto fault, Colton and San Bernardino, southern California; preliminary results: Geological Society of America Abstracts with Programs, v. 37, no. 7, p. 559.

Lozos, J., 2016, A case for historic joint rupture of the San Andreas and San Jacinto faults: Science Advances, v. 2, e1500621, https://doi.org/10.1126/sciadv.1500621.

Machette, M., Haller, K., and Wald, L., 2004, Quaternary Fault and Fold Database for the Nation: U.S. Geological Survey Fact Sheet 2004–3033, https://earthquake.usgs.gov/hazards/qfaults/ (last accessed 15 February 2018).

Marliyani, G.I., Rockwell, T.K., Onderdonk, N.W., and McGill, S.F., 2013, Straightening of the northern San Jacinto fault, California, as seen in the fault-structure evolution of the San Jacinto stepover: Bulletin of the Seismological Society of America, v. 103, no. 3, p. 2047–2061.

McGill, S., Dergham, S., Barton, K., Berney-Ficklin, T., Grant, D., Hartling, C., Hobart, K., Minnich, R., Rodriguez, M., Runnerstrom, E., Russell, J., Schmoker, K., Stumfall, M., Townsend, J., and Williams, J., 2002, Paleoseismology of the San Andreas fault at Plunge Creek, near San Bernardino, southern California: Bulletin of the Seismological Society of America, v. 92, p. 2803–2840, https://doi.org/10.1785/0120000607.

McGill, S., Owen, L., Weldon, R., and Kendrick, K., 2013, Latest Pleistocene and Holocene slip rate for the San Bernardino strand of the San Andreas fault, Plunge Creek, southern California: Implications for strain partitioning within the southern San Andreas fault system for the last 35 k.y.: Geological Society of America Bulletin, v. 125, p. 48–72, https://doi.org/10.1130/B30647.1.

McGill, S., Spinler, J., McGill, J., Bennett, R., Floyd, M., Fryxell, J., and Funning, G., 2015, Kinematic modeling of fault slip rates using new geodetic velocities from a transect across the Pacific–North America plate boundary through the San Bernardino Mountains: Journal of Geophysical Research, v. 120, p. 2772–2793.

Morton, D.M., and Matti, J.C., 1993, Extension and contraction within an evolving divergent strike-slip fault complex; the San Andreas and San Jacinto fault zones at their convergence in southern California, *in* Powell, R.E., Weldon, R.J., and Matti, J.C., eds., The San Andreas Fault System: Displacement, Palinspastic Reconstruction, and Geologic Evolution: Geological Society of America Memoir 178, p. 217–230, https://doi.org/10.1130/MEM178-p217.

Oglesby, D., 2005, The dynamics of strike-slip step-overs with linking dip-slip faults: Bulletin of the Seismological Society of America, v. 95, p. 1604–1622, https://doi.org/10.1785/0120050058.

Onderdonk, N., Rockwell, T., McGill, S., and Marliyani, G., 2013, Evidence for seven surface ruptures in the past 1600 years on the Claremont fault at Mystic Lake, northern San Jacinto fault zone, California: Bulletin of the Seismological Society of America, v. 103, p. 519–541, https://doi.org/10.1785/0120120060.

Onderdonk, N., McGill, S., and Rockwell, T., 2015, Short-term variations in slip rate and size of prehistoric earthquakes during the past 2000 years on the northern San Jacinto fault zone, a major plate-boundary structure in southern California: Lithosphere, v. 7, p. 211–234, https://doi.org/10.1130/L393.1.

Oskin, M., Elliot, A., Duan, B., Liu-Zeng, J., Liu, Z., Shao, Y., Prush, V., Morelan, A., Chester, J., and Elizondo, D., 2015, Earthquake gates: Linking rupture length to geologically constrained dynamics of fault complexity, with examples from the Altyn Tagh and San Andreas faults: Geological Society of America Abstracts with Programs, v. 47, no. 7, p. 35.

Philibosian, B., Fumal, T., and Weldon, R., 2011, San Andreas fault earthquake chronology and Lake Cahuilla history at Coachella, California: Bulletin of the Seismological Society of America, v. 101, p. 13–38, https://doi.org/10.1785/0120100050.

Plesch, A., Shaw, J.H., Bryant, W.A., Carena, S., Cooke, M.L., Dolan, J.F., Fuis, G.S., Gath, E.M., Grant Ludwig, L.B., Hauksson, E., Jordan, T.H., Kamerling, M.J., Legg, M.R., Lindvall, S.C., Magistrale, H., Nicholson, C., Niemi, N.A., Oskin, M.E., Perry, S.C., Planansky, G., Rockwell, T.K., Shearer, P.M., Sorlien, C.C., Suess, M., Suppe, J., Treiman, J.A., and Yeats, R.S., 2007, Community Fault Model (CFM) for Southern California: Bulletin of the Seismological Society of America, v. 97, p. 1793–1802, https://doi.org/10.1785/0120050211.

Pollitz, F., and Sacks, I., 1992, Modeling of postseismic relaxation following the great 1957 earthquake, southern California: Bulletin of the Seismological Society of America, v. 82, p. 454–480.

Prescott, W.H., Savage, J.C., Svarc, J.L., and Manaker, D., 2001, Deformation across the Pacific–North America plate boundary near San Francisco, California: Journal of Geophysical Research, v. 106, p. 6673–6682, https://doi.org/10.1029/2000JB900397.

Reimer, P., Bard, E., Bayliss, A., Beck, J., Blackwell, P., Bronk Ramsey, C., Grootes, P., Guilderson, T., Haflidason, H., Hajdas, I., Hatté, C., Heaton, T., Hoffmann, D., Hogg, A., Hughen, K., Kaiser, K., Kromer, B., Manning, S., Niu, M., Reimer, R., Richards, D., Scott, E., Southon, J., Staff, R., Turney, C., and van der Plicht, J., 2013, IntCal13 and Marine13 radiocarbon age calibration curves 0–50,000 years cal BP: Radiocarbon, v. 55, p. 1869–1887, https://doi.org/10.2458/azu_js_rc.55.16947.

Rockwell, T., Dawson, T., Ben-Horin, J., and Seitz, G., 2015, A 21 event, 4,000-year history of surface ruptures in the Anza seismic gap, San Jacinto fault: Implications for long-term earthquake production on a major plate boundary fault: Pure and Applied Geophysics, v. 172, p. 1143–1165, https://doi.org/10.1007/s00024-014-0955-z.

Rockwell, T., Scharer, K., and Dawson, T., 2016, Earthquake geology and paleoseismology of major strands of the San Andreas fault system, *in* Anderson, R., and Ferriz, H., eds., Applied Geology in California: Redwood City, California, Star Publishing, p. 721–756.

Salisbury, J.B., Rockwell, T.K., Middleton, T.J., and Hudnut, K.W., 2012, LiDAR and field observations of slip distribution for the most recent surface ruptures along the central San Jacinto fault: Bulletin of the Seismological Society of America, v. 102, p. 598–619, https://doi.org/10.1785/0120110068.

Sanders, C., 1993, Interaction of the San Jacinto and San Andreas fault zone, southern California: Triggered earthquake migration and coupled recurrence intervals: Science, v. 260, p. 973–976, https://doi.org/10.1126/science.260.5110.973.

Scharer, K.M., Biasi, G.P., Weldon, R.J., II, and Fumal, T.E., 2010, Quasi-periodic recurrence of large earthquakes on the southern San Andreas fault: Geology, v. 38, no. 6, p. 555–558, https://doi.org/10.1130/G30746.1.

Sedki, Z., 2013, LiDAR and Field Investigation Along the San Andreas Fault, San Bernardino/Cajon Pass Area, Southern California [M.S. thesis]: Long Beach, California, California State University, 91 p.

Seitz, G., Weldon, R., and Biasi, G., 1997, The Pitman Canyon paleoseismic record: A re-evaluation of southern San Andreas fault segmentation: Journal of Geodynamics, v. 24, p. 129–138, https://doi.org/10.1016/S0264-3707(96)00042-7.

Sieh, K., and Jahns, R.H., 1984, Holocene activity of the San Andreas fault at Wallace Creek, California: Geological Society of America Bulletin, v. 95, p. 883–896, https://doi.org/10.1130/0016-7606(1984)95<883:HAOTSA>2.0.CO;2.

Spinler, J., Bennett, R., Anderson, M., McGill, S., Hreinsdottir, S., and McCallister, A., 2010, Present-day strain accumulation and slip rates associated with southern San Andreas and Eastern California shear zone faults: Journal of Geophysical Research, v. 115, p. 2156–2202, https://doi.org/10.1029/2010JB007424.

Thatcher, W., 1979, Systematic inversion of geodetic data in central California: Journal of Geophysical Research, v. 84, p. 2283–2295, https://doi.org/10.1029/JB084iB05p02283.

Toppozada, T., Branum, D., Reichle, M., and Hallstrom, C., 2002, San Andreas fault zone, California: $M \geq 5.5$ earthquake history: Bulletin of the Seismological Society of America, v. 92, p. 2555–2601, https://doi.org/10.1785/0120000614.

Wells, D., and Coppersmith, K., 1994, New empirical relationships among magnitude, rupture length, rupture width, rupture area, and surface displacement: Bulletin of the Seismological Society of America, v. 84, p. 974–1002.

Wesnousky, S., 2006, Predicting the endpoints of earthquake ruptures: Nature, v. 444, p. 358–360, https://doi.org/10.1038/nature05275.

Yule, D., and Sieh, K., 2001, The paleoseismic record at Burro Flats: Evidence for a 300-year average recurrence for large earthquakes on the San Andreas fault in San Gorgonio Pass, southern California: Geological Society of America Abstracts with Programs, v. 33, no. 3, p. 31.

Yule, D., and Sieh, K., 2003, Complexities of the San Andreas fault near San Gorgonio Pass: Implications for large earthquakes: Journal of Geophysical Research, v. 108, 2548, https://doi.org/10.1029/2001JB000451.